Effects of H₂SO₄, HCl, and MgSO₄ Attack on Porcelain-Based Geopolymer Concrete

Rada Klingsad [1], Borvorn Israngkura Na Ayudhya [1*]

[1] *Department of Civil Engineering, Faculty of Engineering, Rajamangala University of Technology Thanyaburi, Pathum Thani, 12110, Thailand.*

Abstract

This study examined the durability of porcelain-based geopolymer concrete when exposed to strong acids, chlorides, and sulfates. Specimens prepared with a 14M NaOH solution and initially cured at 105°C for 24 hours were submerged in acidic and alkaline solutions for varying durations—3, 7, 14, 21, 28, 60, and 90 days. Compressive and splitting tensile strength tests were conducted to assess material performance. The results showed that immersion in H_2SO_4, HCl, and $MgSO_4$ solutions led to weight loss and reductions in both compressive and splitting tensile strengths. Strength deterioration was more pronounced in the early stages, with a peak weight loss rate of 15.32 g/day. After 90 days in 20% H_2SO_4, 20% HCl, and 20% $MgSO_4$ solutions, the residual compressive strengths were measured at 2.80, 14.19, and 3.29 N/mm², respectively, while splitting tensile strengths were recorded at 0.40, 1.21, and 0.51 N/mm². The ratio of splitting tensile strength to compressive strength (f_{sp}/f'_c) was influenced by molar concentration and immersion duration. Experimental findings revealed that a high molarity NaOH solution and elevated curing temperature enhanced resistance to HCl attack more effectively than H_2SO_4 and $MgSO_4$. Moreover, the experimental data closely aligned with the ACI 318 design code, though it tended to overestimate tensile strength.

Keywords: Geopolymers; Porcelain; Chemical Resistance; Splitting Tensile Strength.

1. Introduction

The rise in living standards has led to increased product manufacturing and waste generation. Additionally, higher energy costs, raw material expenses and global competition have further driven up production costs [1]. While investing in environmentally friendly processes or developing innovative technologies is a costly and long-term commitment, minimizing the environmental impact of sanitary ware porcelain production remains a key concern for the industry [2]. Sustainability in manufacturing is among the most widely discussed topics regarding environmental impact [3]. Sanitary ware porcelain production generates significant waste at various processing stages. Studies have explored the use of porcelain products in construction applications, along with waste and defective materials. One effective strategy for reducing waste and landfill costs is incorporating sanitary ware porcelain waste into concrete mixtures [4-7]. Unwanted or defective porcelain products make up approximately 5–10% of total production volume. Replacing Ordinary Portland Cement (OPC) with geopolymer binders in concrete structures offers a sustainable solution for creating durable materials that resistant to environmental degradation. Geopolymer binders present two primary environmental benefits over OPC. First, lowering greenhouse emissions during production. Second, repurposing industrial by-products or defective materials as binder components. Sanitary ware porcelain, which is low in CaO but high in SiO_2 and Al_2O_3, can serve as an effective geopolymer binder. Geopolymer concrete outperforms conventional ordinary concrete in several aspects,

including chemical resistance [8-10], thermal resistance [11-12], and low shrinkage and expansion [13]. Additionally, the corrosion durability of geopolymer concrete has been investigated by several researchers. Miranda et al. [14] found that fly ash based geopolymer mortar exhibited corrosion resistance comparable to cement mortar when exposed to a high molarity NaOH solution (14M).

Kupwade-Patil & Allouche [15] demonstrated that fly ash type C showed better resistance to chloride ingress than fly ash type F after one year of exposure to wet-dry cycles in 7.5% sodium chloride Chindaprasirt & Chalee [16] showed that higher NaOH molarity enhanced compressive strength and reduced chloride penetration in fly ash based geopolymer concrete after three years in a marine environment. Noushini & Castel [17] found that optimized curing conditions decreased permeable void volume while increasing electrical resitivity and compressive strength. These studies suggest that utilizing a high molarity NaOH solution and increasing the sodium silicate-to-sodium hydroxide ratio above 2.5 accelerates the geopolymerization process; Greater concentrations of both NaOH solution and sodium silicate (Na_2SiO_3) improve the passivity of geopolymer concrete. Reddy et al. [18] reported that fly ash class C-based geopolymer concrete enhanced resistance against chloride environments compared to conventional concrete. Similar results were also found by Olivia & Nikraz [19]. The chemical resistance of geopolymer was directly related to its permeability and porosity, which affected how alkali solutions are transported. The severity of chemical attacked on specimens depended on the level of alkali concentration, initial curing temperature, and velocity of the solution. Therefore, a less permeable matrix in specimens provided greater resistance to chemical attack [20]. Aldawsari & Kampmann [21] reported that low calcium fly ash mixed with slag binder reduced weight loss of up to 7% and improved in compressive strength by 6-16% under a 5% sulfate solution attack compared to ordinary Portland cement. Sing et al [22] demonstrated that usage of ternary material binder (fly ash type F mixed with silica fume and ground granulated blast furnace slag) in geopolymer concrete increased durability and compressive strength while reducing mass loss under 5% H_2SO_4 attack environment.

Bai et al. [23] showed that binary (red mud slag and solid waste incineration fly ash) binder material exhibited higher acid resistance to sulfuric attack compared OPC. The compressive strength loss was 20% after 112 days of exposure to acid environment. To improve mechanical and chemical resistance of structure, porcelain has emerged in the form of geopolymer binder which enhanced resistance to sulfate and acid attack due to their ceramic-like microstructure. Berkouche et al. [24] found that increasing ceramic waste powder improved workability and long term compressive strength of 86.34 N/mm^2 at 28 days. Abdelmonem et al. [25] investigated the durability of ceramic waste powder (CWP) based geopolymer specimens after exposure to marine conditions. The results revealed that using 20% of CWP in geopolymer mixture is suitable for fully submerged structures in marine, while 15% of CWP based geopolymer specimens are fit for normal conditions. In terms of abrasive resistance, Mohebi et al. [26] studied alkali-activated slag-based geopolymer concrete. The results showed that curing temperature at 60°C and 95°C improved abrasive wear performance of geopolymer concrete. However, Yan et al. [27] demonstrated that extension of curing time decreased abrasion wear resistance of fly ash-based geopolymer concrete. Luhar et al. [28] presented the results of abrasion resistance of fly ash-based geopolymer concrete with rubber fibers. They found that the abrasion resistance of OPC and geopolymer concrete was similar without the use of fibers. Witzke et al. [29] found that the usage of low calcium material (metakaolin) as binding material in geopolymer concrete gave the same or better result in abrasion resistance performance than that of Portland cement concrete. Noushini et al. [30] reported that metakaolin and metakaolin mixed with rice husk ash-based geopolymer concrete exhibited good performance, with substantially less wear. Arslan et al. [31] explored the abrasion resistance of high calcium binder materials-based geopolymer concrete mixed with fibers. Results showed that abrasion resistance increased with the incorporation of PVA fibers and basalt fibers.

As concerns grow regarding the environmental impact of construction materials and the high long-term maintenance costs of structures exposed to acid, chloride, and sulfate attacks, ordinary Portland cement faces significant durability challenges. Studies have examined sulfate, chloride and acid attacks on low-calcium-based geopolymer binder systems. However, limited research has specifically focused on the chemical resistance of low-calcium-content materials, particularly porcelain-based geopolymer binder. This might be due to the difficulties in the preparation stage of making porcelain powder. The hardness of porcelain is above 7, requiring extra time for hammering, grinding and cutting the raw material. In order to encouraged the usage of industrial waste and less expensive binder, this study aimed to extent the clarification of the effect of H_2SO_4, HCl and $MgSO_4$ at difference concentration levels (5%, 10%, 15%, and 20%) on the mechanical properties and durability of porcelain-based geopolymer concrete. The immersion duration was governed at 3, 7, 14, 21, 28, 60 and 90 days. The properties were characterized by visual appearance, mass loss, compressive and splitting tensile strength. SEM, XRF and XRD were chosen to analyze the mechanism of acid and alkaline corrosion resistance for porcelain based geopolymer concrete.

2. Experiment Methods

2.1. Materials

In this study, defected sanitary ware porcelain powder was used as a precursor material in the geopolymer mixes. Figure 1. showed dry materials used in this study. For aggregates, inland sand and limestone were used as fine and coarse aggregate respectively. The particle size of fine aggregate was lesser than 0.475 mm. The specific gravity in SSD

condition and water absorption of the fine aggregate were 2.67 and 0.24% respectively. The size of coarse aggregate was in the range of 9-12 mm. The maximum size aggregate was 12 mm. The particle size of the porcelain powder was passed through sieve No. 200 (<75 μm). Scanning electron microscopy (JSM-IT500HR model) was used to analyze the morphology of the porcelain. Scanning electron microscopy (SEM) images of the porcelain powder were given in Figure 2. All micrographs were taken at 500X and 20,000X magnification respectively. Under high magnification, the surface of the porcelain particles was revealed. The particles were not rounded. This was due to the preparation process of the porcelain powder, where the porcelain was hammered and cut by rotating blade machine. Figure 3. illustrated the preparation process of sanitary ware porcelain powder. The waste granular porcelain material was washed and oven dried for 24 hour. The dried raw porcelain was cut using a rotating blade machine at a high shear rate for 5 min. The porcelain was then sieved to classify and grade the particle size. The particle shape was angular with sharp edges. The surface of the particles was not smooth. This might affect the transportability of the particles in the geopolymer matrix during mixing and placing. To minimize both internal friction (between mixing materials) and external friction (between the geopolymer matrix and the mold), a superplasticizer (SP) was required. In this study, polycarboxylates used in the mixture. The high-range water reducing admixture helped to improve rheological performance of fresh porcelain based geopolymer. The dosage of SP was 1.0 % by porcelain weight. The porcelain powder was also subjected to X-ray fluorescence (XRF). The chemical composition of the porcelain was shown in Table 1. A Bruker model S8 Tiger series was used in a vacuum atmosphere.
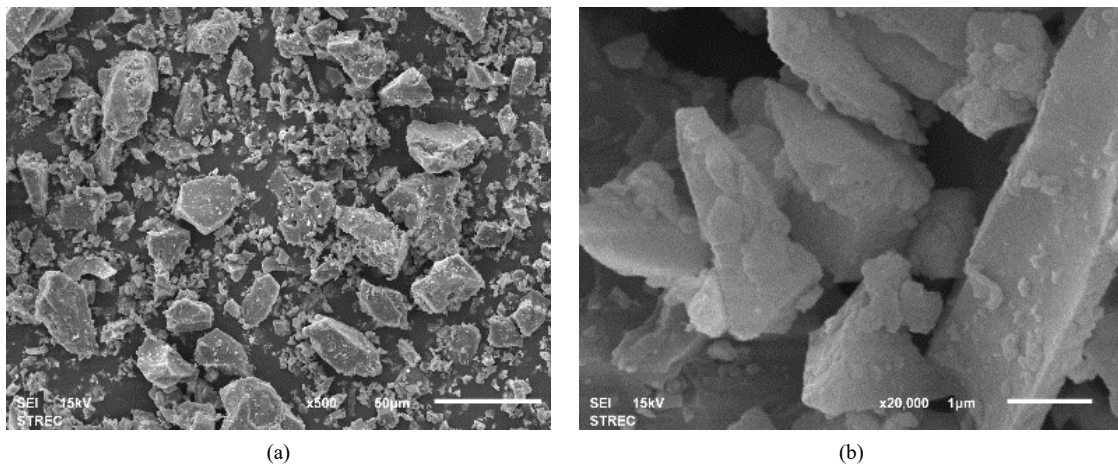

Figure 1. Dry material used in this study

(a)   (b)

Figure 2. SEM particle images of (a) Porcelain at 500X (b) Porcelain at 20,000X
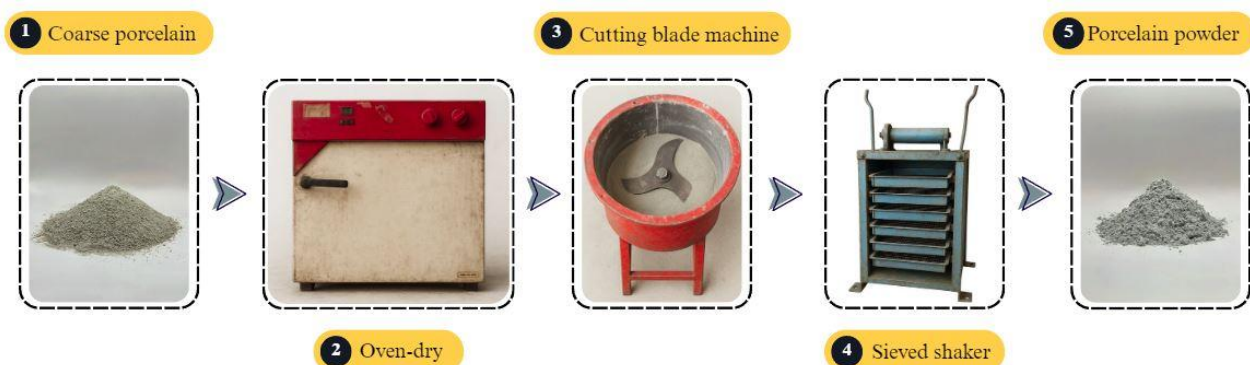

Figure 3. The preparation porcelain powder used in this study

Table 1. Chemical analysis and physical properties of defected sanitary porcelain and OPC material

Oxides	Porcelain (%)	Cement (%)
CaO	2.78	63.43
SiO_2	55.90	17.82
Al_2O_3	17.61	3.78
SO_3	0.01	2.88
Fe_2O_3	1.62	2.77
MgO	0.48	1.81
K_2O	3.06	0.42
TiO_2	0.21	0.30
Na_2O	1.12	0.24
Others	8.11	3.94
LOI	9.10	2.61
Physical properties		
Particle size		
D_{10}	2.02	3.34
D_{50}	17.2	12.3
D_{90}	51.9	32.8
Weight residual	0.83	0.38
Specific gravity		2.64

For the activator, two main chemical substances were used. The activating solution for the geopolymer was sodium silicate (waterglass), which was in liquid form solution (Na_2SiO_3) with 11.67% Na_2O, 28.66% SiO_2, and 59.67% H_2O. Meanwhile, the sodium hydroxide (NaOH) solution was prepared from sodium hydroxide pellets (NaOH, 99.9%). The mass of the sodium hydroxide solids was expressed in terms of molarity (M). Sodium hydroxide solutions with concentrations of 14M was prepared. Different amounts of sodium hydroxide pellets were initially diluted with de-ionized water to prepare the sodium hydroxide solution. The solution was left to cool for 24 hours, then it was added to a sodium silicate solution to prepare the final alkaline solution with mass ratios of $SiO_2:Na_2O$ as listed in Table 2. The ratio of sodium silicate to sodium hydroxide was fixed for all mixtures.

Table 2. Specimens compositions

Code	NaOH (M)	Solid content (%)	AAS Ratio	Materials (kg/m³)						Curing temperature (°C)
				NaOH	Na_2SiO_3	Porcelain	Coarse aggregate	Fine aggregate	SP	
GPC14	14	52.5	2.5	110	275	550	962	384.78	5.5	105

2.2. Mix Proportions

The mix quantities of porcelain-based geopolymer mixes were presented in Table 2. The NaOH solution molarity was fixed at 14M. In this preparation stage, the alkaline solution was prepared 24 hours before the mixing of geopolymer concrete. For the NaOH solution, NaOH pellets were dissolved in water as per the required molarity. The sequence of mixing involved first pouring the coarse and fine aggregates and porcelain powder into the mixing pan and stirring for 2 minutes. The prepared alkaline solution was then poured into the mix, and wet mixing continued for 3 minutes to obtain fresh porcelain-based geopolymer concrete.

2.3. Details of Specimen Preparation and Curing Methods

After mixing, the fresh specimen mixes were poured into cylindrical molds (100×200 mm) in three layers. Each layer was compacted randomly by tamping with a rod 25 times. Once hand compaction was completed, a vibration table was used to ensure full compaction. The vibration time was 30 seconds. Two different curing regimes were applied to all specimens. First, heat curing in an oven to stimulate the geopolymerization process. Specimens were placed and cured in an oven at 105°C for 24 hours. Second, air curing, where specimens were air-cured for 28 days. Specimens were wrapped with polyethylene film and kept at ambient temperature (32°C±1) and humidity conditions (approximately 75%) until the submersion testing day. All air-cured specimens were fully submerged in various acid and alkaline solutions for 7, 14, 21, 28, and 60 days. Sulfuric acid (H_2SO_4), hydrochloric acid (HCl), and magnesium sulfate ($MgSO_4$) solutions at 5%, 10%, 15%, and 20% concentrations were used as various acid and alkaline environments. The acid and sulfate solutions were renewed every 6 and 3 months, respectively, and the pH was periodically monitored and controlled every month.

2.4. Details of Experiment Methods

2.4.1. Physical Properties of Porcelain Geopolymer Concrete

For the alkali corrosion resistance test, all surfaces of the porcelain concrete specimens were cleaned with sandpaper. This helped to remove grease and reduce the uneven surface of the specimens. After the immersion was completed, the specimens were air-dried for 2 hours. The mass of the submerged specimens was then weighed with an accuracy of 1 g and a range of 30 kg. The loss in weight of the cylindrical specimens was calculated according to the following Equation 1:

$$\text{Mass Loss (\%)} = \left(\frac{m_o - m_a}{m_o}\right) \times 100 \tag{1}$$

where m_o is Mass of test specimen before immersion (mg), m_a is Mass of test specimen after immersion (mg).

In addition, all submerged specimens were also subjected to diameter measurement. A digital display Vernier calipers was used to present the measurement results. The diameter of each specimen was measured at three spaced positions. First and second, the diameters at both ends were taken, with the measurement positions 30 mm away from each end. Third, the measurement was taken at 100 mm from both ends. The corrosion depth of the cylindrical specimens was calculated according to the following Equation 2:

$$\text{Corrosion depth} = \left(\frac{d_a - d_o}{2}\right) \tag{2}$$

where d_o is Diameter of test specimen before immersion (mm), d_a is Diameter of test specimen after immersion (mm).

The penetration of alkali ingress into the specimens was also recorded. All cylindrical specimens of 100×200 mm were sliced into 100×50 mm thick cylinders. The neutralization depth of the specimens was measured by spraying a 1% phenolphthalein indicator on the sliced surface of the specimens. The distance between the edge of the specimen and the discoloration boundary was measured using a digital Vernier caliper.

2.4.2. Mechanical Properties of Porcelain Geopolymer Concrete

Figure 4. showed a schematic of the process methodology applied in this study. Cylindrical specimens of 100×200 mm were used to prepare for compressive and splitting tensile tests. The strengths were evaluated and compared after the specimens were fully submerged in various acid and alkaline concentrations. The period of submersion in alkaline environments was set at 3, 7, 14, 21, 28, 60, and 90 days. However, all submerged specimens were air-dried for 2 hours before testing proceeded. Before the specimens were subjected to the compressive strength test, they were capped flat on both ends using sulfur as the capping material. Capping the ends of the specimens provided plane surfaces perpendicular to the specimen axis to evenly distribute loading forces. A compressive testing machine (Technotest with a capacity of 3000 kN) was used to deliver the compressive strength results.
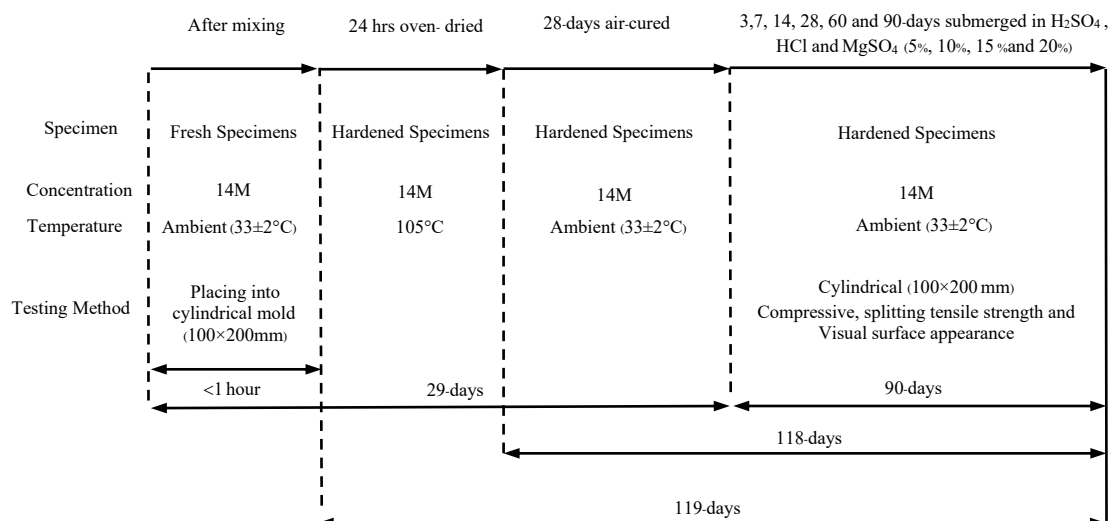

Figure 4. Schematic of process methodology

For splitting strength (ASTM C496/C496M-11) [32], the average result of three specimens was used. The specimen was subjected to a compressive load between two plates. A cylindrical specimen was placed diametrically, leading the cylindrical specimen to fail and split vertically.

For the compressive strength test (ASTM C 39/C39M-99) [33], the cylindrical specimen was applied a compressive axial load until failure occurred. The compressive strength was calculated by dividing the maximum load by the cross sectional area of the specimens (10×20 mm).

3. Results and Discussion

3.1. Chemical Analysis

3.1.1. X-Ray Fluorescence Spectroscopy

The chemical composition and mineralogical phase analysis of porcelain-based geopolymer concrete was conducted using X-ray fluorescence analysis. To study the alteration of chemical composition under various chemical immersions, the specimens were kept in sealed-barrel containers with various concentrations of H_2SO_4, HCl, and $MgSO_4$. The results of the analysis were shown in Table 3. For porcelain binder, it appeared that high concentrations of acid and sulfate environments did not cause significant chemical compound degradation. However, the acidity of sulfuric acid caused the ejection of aluminum from the Si-O-Al bonds of the binder [34], resulting in the weakening, softening, and disintegration of the bonding strength of the alkaline-activated solution [35]. The depolymerization of aluminosilicate polymers and the liberation of silicic acid affected the ability to resist acid corrosion.

The main detected oxides were SiO_2, CaO, and Al_2O_3, respectively. In the sulfate environment, it was found that the level of SO_3 significantly increased compared to the non-chemical immersion specimen. This was due to the precipitation and solution ingress of sulfate into the specimens. Similarly, in the chloride environment, the level of Cl detected was higher than in the non-chemical submersion specimen, due to solution ingress into the specimen. In this study, the XRF analysis of the Mg specimen depicted a moderately high amount of Mg and a high SO_3 concentration in the matrix of the specimens. This evidence demonstrated the migration of magnesium and sulfur ions into the geopolymer concrete specimens, while Na ions were detected at low levels in H_2SO_4, due to the migration of Na ions into the acid solution. Similar findings were reported by Bakharev [9] and Patrisia et al. [36].

Table 3. Major oxides content of porcelain based geopolymer concrete submerged in acid and sulfate at 60 days

Acid and sulfate solution	Oxides								
	CaO	SiO_2	Al_2O_3	Na_2O	MgO	K_2O	Fe_2O_3	SO_3	Cl
Non-chemical submersion	25.32	45.38	5.17	3.77	2.84	1.07	0.86	757 ppm	94.8 ppm
H_2SO_4 (20% concentration)	26.42	46.20	4.62	0.83	0.85	0.70	0.55	9.96	106 ppm
$MgSO_4$ (20% concentration)	24.44	46.50	4.59	5.29	2.67	1.44	1.13	9.67	117 ppm
HCl (20% concentration)	27.93	44.23	4.30	3.18	2.40	0.86	0.67	0.11	0.76

3.1.2. X-Ray Diffraction

The XRD analysis of porcelain-based geopolymer concrete specimens was conducted using a Bruker AXS model D8 Discover. The XRD patterns for porcelain-based geopolymer concrete submerged in acid and sulfate environments are shown in Figure 5 to 7. The phase identification of hardened geopolymer concretes was based on XRF results and the expected reaction products. Peaks detected in the XRD patterns consisted of reacted phases from porcelain and calcium additives such as quartz (SiO_2), calcite ($CaCO_3$), calcium oxide (CaO), graphite, gypsum ($CaSO_4 \cdot 2H_2O$), mullite, merwinite ($Ca_3Mg(SiO_4)_2$), and trace oxide minerals. Figure 7 showed that the exposure of porcelain binder material to sulfuric acid caused the formation of gypsum, and XRD confirmed the increase of sulfur due to the reaction with sulfuric acid. A similar result was found in low-calcium fly ash [37]. The durability of low-calcium binders against acid attack was primarily determined by their chemical and phase composition. A lower calcium content and a higher concentration of hydration products enhanced resistance to deterioration. This occurred because calcium reacted with acetic acid, forming a gel-like precipitate, while the soluble calcium acetate migrated out the matrix paste [38].

The analysis of the residual specimens submerged in HCl using XRD revealed that mullite and quartz remained during the hydrochloric acid attack. In the sulfate environment, the XRD pattern of porcelain-based geopolymer specimens showed a substantial amorphous phase with some peaks of quartz, calcite, mullite, and merwinite. The mullite amorphous phases and quartz alpha (Q) were the main crystalline hydrated phases. The high-intensity 2θ values of porcelain were in the range of 5°-80°. It exhibited that the intensity of porcelain decreased when the calcination and geopolymerization process was completed. This might be due to the amorphous phase of porcelain after geopolymerization [39-41].
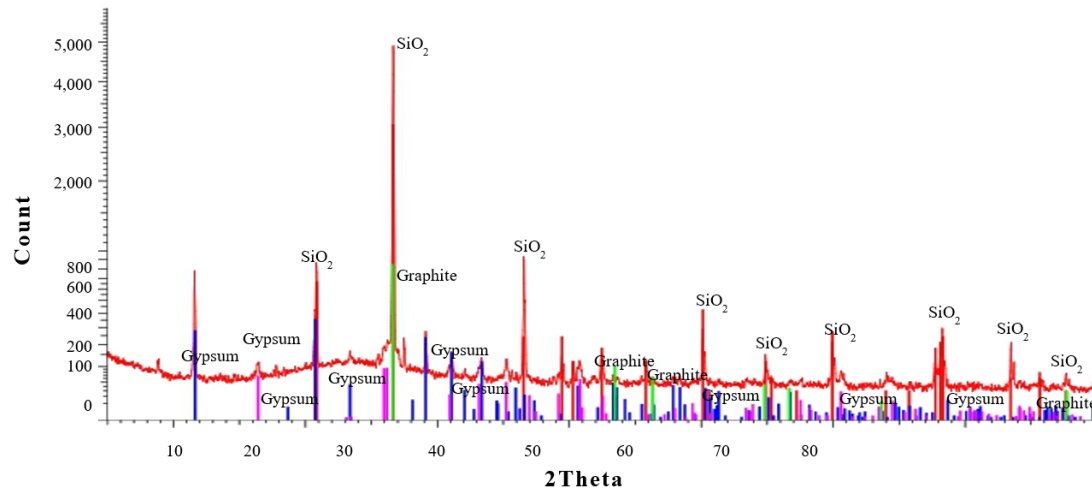
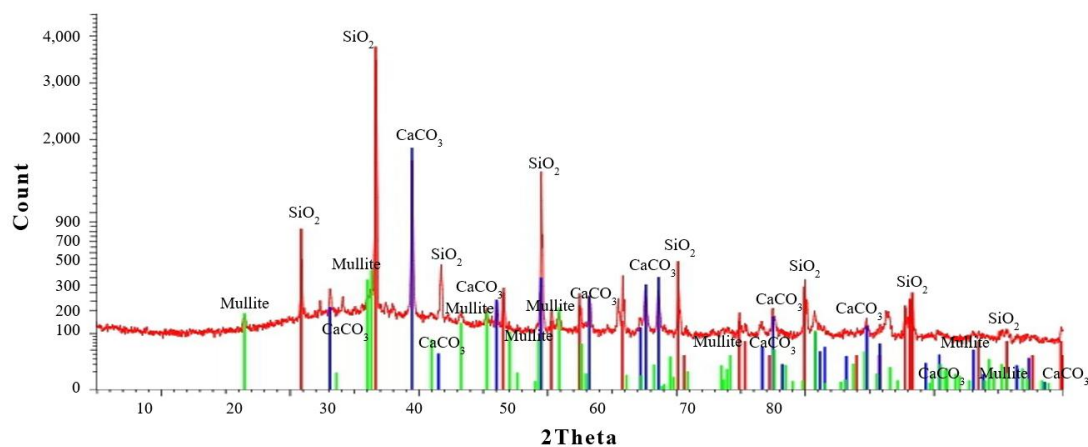**Figure 5. XRD analysis of 14M specimen heat at 105 ºC and submerged in 20% H2SO4 for 60 days**

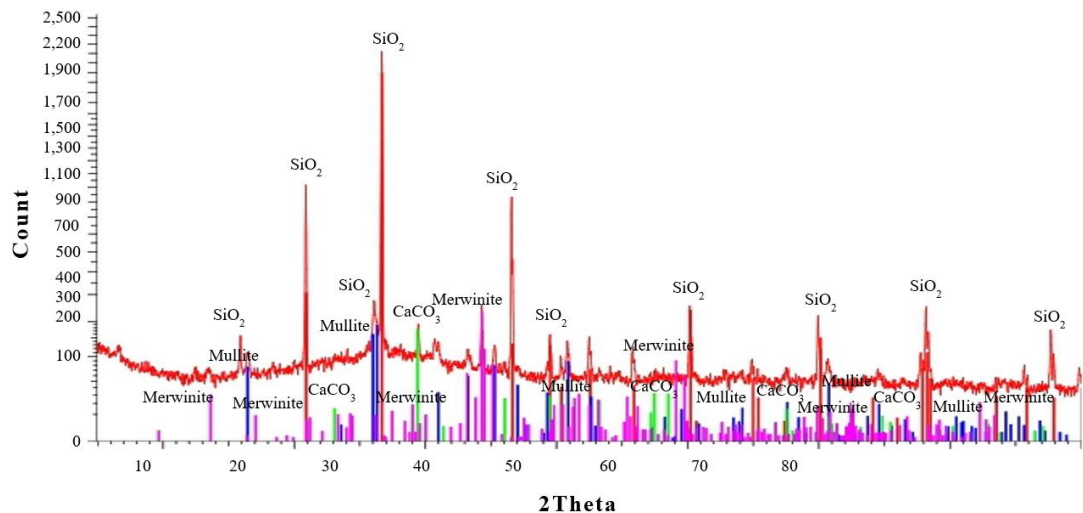**Figure 6. XRD analysis of 14M specimen heat at 105 ºC and submerged in 20% HCL for 60 days**

Figure 7. XRD analysis of 14M specimen heat at 105 ºC and submerged in 20% MgSO4 for 60 days

3.2. Visual Appearance

The changes in the appearances of submerged porcelain-based concrete specimens were noticed and are shown in Figure 8. The changes in the appearances of the specimens depended on the type and concentration of the solution used. In this study, the levels of acid, sulfate, and chloride concentrations used were 5%, 10%, 15%, and 20%. Observations were made on the color surface and specimen profile. Specimens were compared over different periods of immersion. The changing appearance of the specimens was compared using photographs. It was observed that the color appearance of the specimens changed from grey to pale-grey as the period of immersion increased.

Type of solution	Immersion duration (days)	Concentration of solution (%)			
		5	10	15	20
H₂SO₄	28				
	60				
	90				
HCl	28				
	60				
	90				
MgSO₄	28				
	60				
	90				

Figure 8. Immersion of specimens in acid and alkali solutions

For the visual appearance of porcelain-based geopolymer concrete specimens subjected to sulfuric acid solution for 28, 60, and 90 days, the surface of the specimens was smooth with sharp edges before submersion. The corrosion damage caused by the acid solution became more aggressive as the submersion time increased. The characteristics of deterioration first started with the formation of crack lines, followed by the surface of the specimens becoming rougher and the edges becoming less sharp. Secondly, soft mud-like peeling and loose aggregate began to be noticed on specimens submerged in 5% H_2SO_4 for 60 days. The characteristics of soft mud-like peeling and loose aggregate played a more dominant role in the deterioration process than the propagation of

crack lines as the submersion time increased. The specimens experienced scaling and mineral leaching from the aluminosilicate gel. The sand particles were exposed due to the loss of paste from the surface and the edges of the specimens appeared rounded.

For the deterioration of HCl specimens, the formation of crack lines started to be noticed when the specimen was submerged in 5% HCl for 28-days. The cracks further expanded unidirectionally toward both ends. As the concentration of the solution increased, the formation of cracks began to proliferate with the immersion duration increased. The specimens experienced less deterioration and underwent lower disintegration compared to H_2SO_4. The specimens underwent deterioration by leaching, which was marked by decolorization. After exposure to HCl, the surface appearance and intrinsic texture of the submerged specimens were lost due to leaching and the deposition of gypsum [42, 43].

For the sulfate solution, it was found that the matrix pores and surface area of specimens submerged in $MgSO_4$ became saturated. Scaling deposition of $MgSO_4$ on specimens started to be found on 5% $MgSO_4$ after 28 days of submersion. At the early stage of immersion, different levels of white precipitation appeared on the surface of the specimens. The scaling deposition heavily increased with the increment of concentration solution and submersion duration. In the middle stage of immersion, swelling, peeling, and cracking on the surface and around the edges of the specimen were noticed, varying with the concentration of the solution. In the final stage of immersion, spalling action took place when the specimen was submerged in 5% $MgSO_4$ for 60 days. The severity of spalling action continued to increase with the increment of concentration solution. It appeared that the damage caused by the increment of concentration solution had a stronger effect on the physical appearance than the submersion duration.

For the specimen profile, the profile of the specimen also changed as the level of solution concentration increased. For H_2SO_4 submersion, the surface of the specimen appeared porous with loose particles. The formation of cracks did not occur. The degree of severity increased with the level of acidity concentration and the period of immersion. The surface of the specimens became more porous with slight peeling. It was also noticed that the surface of the specimens became uneven and rough. However, the structure of the specimens remained intact and dense. The visibility of cracks on the surface of specimens submerged in HCl and $MgSO_4$ occurred when the concentration of the solution was at 15% for 28 days and 5% for 60 days of submersion respectively. The surface became rougher with an increase in open pores. For the $MgSO_4$ profile, the formation of cracks occurred after 28 days of submersion. The surface also became rougher with the attachment of $MgSO_4$ crystals. The pores were also filled with saturated $MgSO_4$, and the open cracks became larger.

The neutralization depth of porcelain-based geopolymer concrete in an acidic environment was also studied. The pH of the specimens decreased as the level of acidic concentration increased. Thus, the equilibrium of pH was changed which chemical compounds of the matrix altered. Calcium carbonate was transformed into soluble bicarbonate, which was depleted by leaching into the acidic solution. The pore size and number of pores then increased due to the reduction and decomposition of calcium to amorphous hydrogel. The crystalline phase formation within the aluminosilicate matrix was important for the stability of geopolymer material in an acidic environment. Additionally, the median pore size of the specimen had a significant effect on its durability [44]. The neutralization depth of submerged specimens increased with exposure to acidic solution time. It found that corrosion depth for 60 days submerged with 5% and 20% H_2SO_4 was in the range of 0.003-0.04 mm and 0.005-0.030 respectively. An increment of penetration of acidic solution in specimens was due to porcelain based geopolymer concrete had a poor resistance to the acidic penetration. The correlation between the corrosion depth and the corrosion time was shown in Figure 9. For sulfate submersion, it observed that an early age of corrosion was taken place when specimen reacted with sulfate solution and expansive white corrosion products were deposited on the surface of specimens. This caused increment in diameter of specimen and corrosion depth.

However, prolonging the submerged time of specimens, the corrosion products were travelled through inside. Consequence, the layer of surface was spalled off. Therefore, the diameter of specimen reduced. Based on the corrosion depth, the degree of damaging to specimen subjected to sulfate could be ranked as moderate severe. A higher alkaline concentration of specimen increased resistance to alkaline corrosion. The neutralization depth of 5% and 20% $MgSO_3$ was in the range of 0.001-0.019 mm and 0.003-0.230 mm respectively. For HCl, chloride crystallization induces expansion, resulting in surface irregularities and increased internal pressure within the pores. Addition, a chemical reaction occurred between the alkaline activator and HCl solution which caused deterioration of constituent materials. The decomposition is severe when concentration of solution increased. The neutralization depth of 5% and 20% was in the range of 0.024-0.103 and 0.05-0.289 mm respectively.

(a) H₂SO₄ (5%)

(b) H₂SO₄ (20%)

(c) HCL (5%)

(d) HCL (20%)

(e) MgSO4 (5%)

(f) MgSO4 (20%)
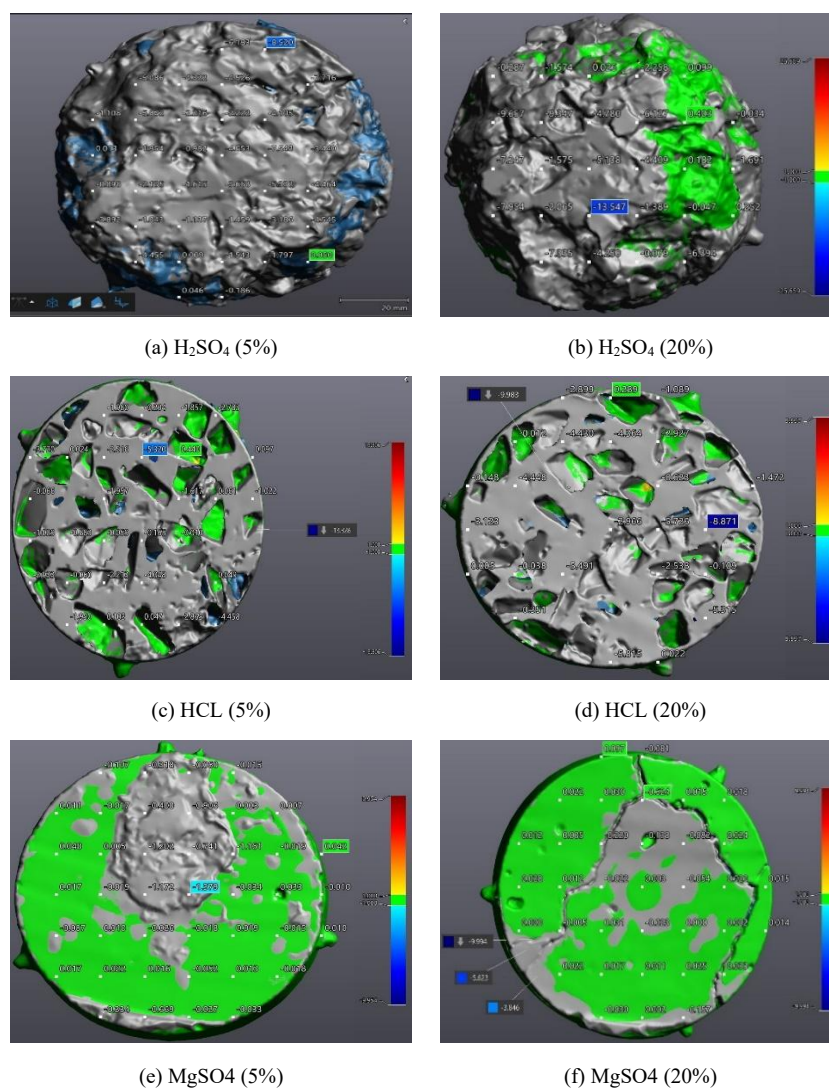
Figure 9. Neutralization depths of specimens

The influence of Si/Al ratio on resistance to acidic, chloride and sulfate attacks on specimens was examined. The defective sanitary ware porcelain powder used in this study had an Si/Al ratio of 3.05, which was significantly high Si/Al ratio where typical fly ash type F had Si/Al ratio ranged 1.6 [45] - 2.10 [46]. The high Si/Al ratio did cause the specimens unhardened under normal environment. Thus, oven-cured was required. The experimental results showed that the leaching damage of porcelain based geopolymer concrete specimens submerged in HCl solutions was insignificantly compared to H₂SO₄ and MgSO₄ (Figure 10) and fly ash type F where specimens appeared completely destructive form [47]. Submerged specimens did not completely unchanged matrix texture. A high Si/Al ratio provided a stable and protective silica-rich layer on the surface of specimen. This layer acted as a barrier, preventing further chemical attack and extending the specimen's lifespan. The specimens exhibited a dense and interconnected microstructure, enhancing their resistance to HCl attack. Whereas, the matrix of specimen submerged in H₂SO₄ solution did show clearly picture of matrix destruction.

The specimens showed severe leaching when specimens were fully submerged after 28 days. H₂SO₄ solution has the ability to destroy the amorphous matrix in specimens even 5% concentration solutions (H₂SO₄ and MgSO₄) were used. It appeared that calcium element were depleted from matrix. The ability to resist acidic of binding materials depended on bonding strength of hydration products and acidic media. For MgSO₄ submerged specimens, a slightly deteriorate from leaching was noticed. Similar results found by others [47, 48] indicated that a high Si/Al ratio in geopolymers enhanced resistance to MgSO₄ attack. This was due to a high Si/Al ratio led to the formation of more stable, less reactive phases within the geopolymer matrix, which can better withstand the damaging effects of magnesium sulfate. Increasing the concentration of MgSO₄ facilitated the incorporation of Si into the specimen, pores diameter and volume were less susceptible to enlargement. Internal micro cracks were lesser to occur. The strength of specimens was not sharply decrease. Additionally, the transfer of Si into the matrix helped counteract the negative effects of reduced alkalinity. Specimens exposed to MgSO₄ solution exhibited phase of brucite and hydrated magnesium gel (M-S-H). This indicated that the specimens exhibited resistance to MgSO₄ attack.

3.3. Development of Strength

3.3.1. Compressive Strength

Figures 10-a and 10-b illustrated the 3, 7, 14, 28, 60, and 90-days compressive strength of porcelain-based geopolymer concretes exposed to H_2SO_4, HCl, and $MgSO_3$ concentrations of 5%, 10%, 15%, and 20%. The compressive strength of specimens in the 5% and 10% H_2SO_4 groups decreased from 37.30 N/mm² to 17.66 N/mm² and from 36.09 N/mm² to 14.14 N/mm² respectively. The results exhibited the highest loss in compressive strength compared to HCl and $MgSO_3$ specimens. The deterioration resulted from the disruption of the oxy-aluminum bridge (Al-Si-O) within the geopolymerization products [49]. The sulfuric acid solution disrupted the chemical reaction and reduced the compressive strength. During period of H_2SO_4 attack to specimens, the alkali-activated porcelain binder exhibited a sign of leaching where most of sodium, calcium and aluminum were leached from the matrix. However, silicon still remained intact.

Therefore, the strengths of the low calcium binder material mainly relied on its silicon-rich structure [50]. In this study, the characteristic of increment in compressive strength before its decline at an early age of submersion was not clearly found. Similar results were found in metakaolin binder [31, 51]. However, it was noted that the loss rate in compressive strength decreased at an early age of immersion (14 days) from 0.63 N/mm² per day to 0.36 N/mm² per day (Figure 11 (a)). The loss rate in compressive strength began to increase after 14 days (0.36 N/mm² per day) until 28 days (0.59 N/mm² per day) of H_2SO_4 immersion. After 28 days, the loss rate in compressive strength started to decline until 90 days. A further noticeable reduction in compressive strength was observed when specimens were exposed to the 15% and 20% H_2SO_4 solutions. The lowest residual compressive strength was found after 90 days of exposure. The lowest residual compressive strength was found after 90 days of exposure. Following 90-days of immersion in 15% and 20% H_2SO_4 solutions, the residual compressive strength was 7.97 N/mm² and 2.80 N/mm² respectively. However, the correlation between H_2SO_4 concentration and strength degradation may not follow a linear trend; further results are needed to reinforce this hypothesis.
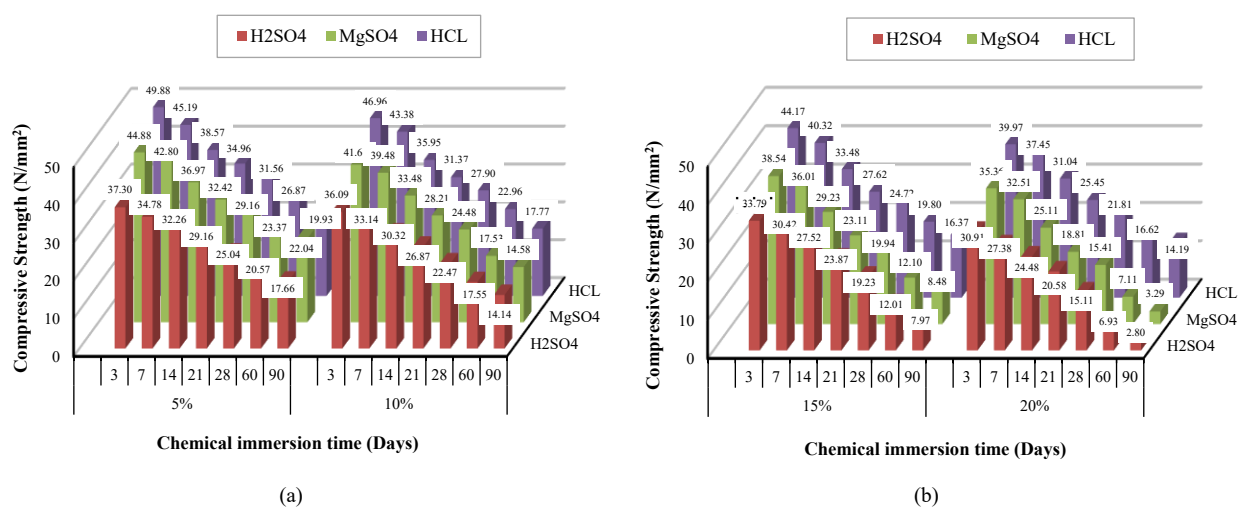
Figure 10. Residual compressive strength of specimens

For HCl, the compressive strength dramatically reduced when the HCl solution was introduced. Following 7-days of immersion in 5% and 10% HCl solutions, the compressive strengths were 45.19 N/mm² and 43.38 N/mm² respectively. It was found that the compressive strength values were generally higher than those of the H_2SO_4 specimens. After 28 days of exposure to 5% and 10% concentrations, the compressive strengths were only 31.56 N/mm² and 27.90 N/mm² respectively. These observations indicated that the deterioration of compressive strength in porcelain-based geopolymer concrete became more severe when submerged in higher concentration solutions. A similar result was found by Wan-en et al. [52]. At an early age of immersion, the deterioration rate of compressive strength was rapid. The deterioration rate decreased as the immersion age increased, and the compressive strength then stabilized. This could be attributed to the solution reaching full saturation, leading to deposition and penetration into the specimen's pores. The resulting precipitation hindered the diffusion of harmful Cl ions. At longer immersion ages (60-days and 90-days) with higher concentrations of solutions (15% and 20%), the compressive strength decreased from 19.80 N/mm² to 16.37 N/mm² and from 16.62 N/mm² to 14.19 N/mm² respectively. In Figure 11-b showed that at 7-days of immersion, the loss rate in compressive strength increased from 0.95 to 0.107 N/mm² per day before the loss rate in compressive strength began to decline towards 90 days of immersion.

(a)

(b)

(c)
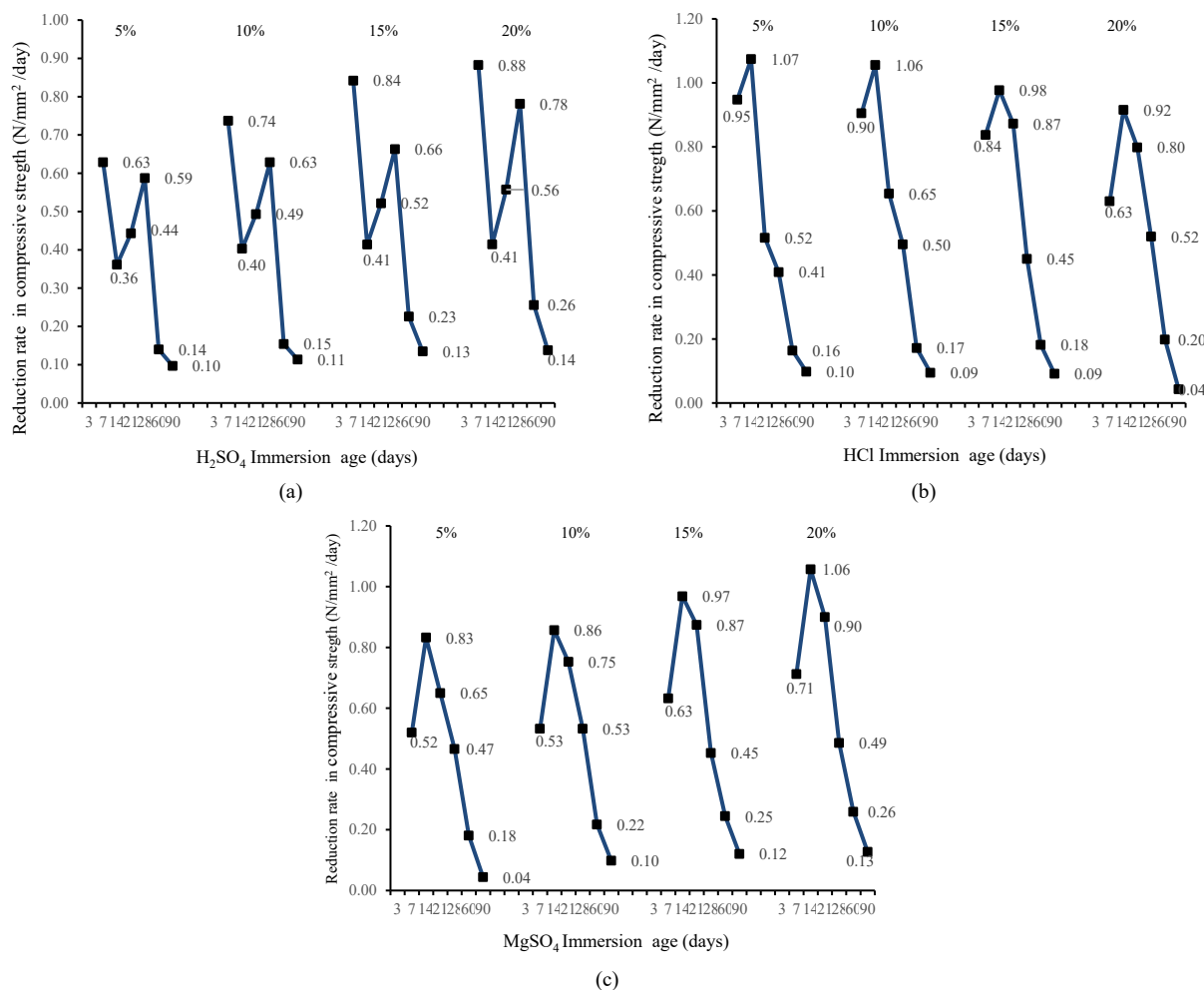
Figure 11. Rate of changing residual compressive strength

For MgSO4, the compressive strength after 7-days (42.80 N/mm²) and 28 days (29.16 N/mm²) of exposure to 5% MgSO4 experienced a compressive strength drop. The pattern of compressive strength deterioration was similar to that observed in HCl specimens (Figure 11-b and Figure 11-c). The severity damage caused by the submerged solution was minor compared to the H2SO4 specimens. However, MgSO3 specimens experienced greater damage than HCl specimens. This resulted from the formation of magnesium aluminum silicate hydrate (M-A-S-H) gel, which had weak bonding strength and was produced by the magnesium sulfate reaction. The degradation mechanism of geopolymers was primarily influenced by the interaction of cations with sulfate anions, which facilitated decalcification and the breakdown of the primary binding phase [53, 54]. The regain in compressive strength was also not found in this study. It appeared that only the rate of deterioration in compressive strength decreased after 14-days of immersion. This might be due to fewer unreacted raw materials for dissolution which promoted continual geopolymerization and compensated for the strength loss from sulfate corrosion [55]. The determination of selecting alkali activators had a great impact on corrosion resistance. At 60-days and 90-days of immersion in 20% concentration, compressive strength values gradually decreased from 7.11 N/mm² to 3.29 N/mm² respectively. Specimens suffered a loss in compressive strength due to sulfate exposure. The strength loss increased as the sulfate concentration increased. The anions (SO-4) ingressed into the geopolymer matrix, the cation (Mg2+) consumed the alkali and precipitated [56]. This caused alkalinity of MgSO4 decreased and compressive strength decreased. It appeared that porcelain-based geopolymer concrete showed superior resistance to magnesium sulfate compared to hydrogen sulfate (sulfuric acid).

Figure12-a to 12-e showed the fractures in residual porcelain based geopolymer concrete specimens. The effect of chemical concentration and immersion period to cracking characteristics of porcelain based geopolymer concrete under compressive stress were studied. In this study, two types of surface crack line on specimen surface were identified. The first crack line type resulted from sulfate and chloride solution precipitated into pores, causing spalling. The second crack line type developed during compressive strength testing. At pre-compressive test, initial crack widths ranged from 0.3-1mm, with crack lines extended along the vertical axis. During compressive loading, secondary crack lines propagated along the first crack lines, growing diagonally toward the specimen ends. Crack lines grew rapidly when load was applied. However, lesser energy required to further extend or fully open crack gaps of high concentration submerged specimens when immersion duration of specimens was longer than 21 days. The bong strength of matrix was ruined by chemical attack.

(a) 3 days in H2SO4   (b) 3 days in HCl   (c) 3 days in MgSO$_4$

(d) 90 days in H$_2$SO$_4$ (e) 90 days in HCl   (f) 90 days in MgSO$_4$
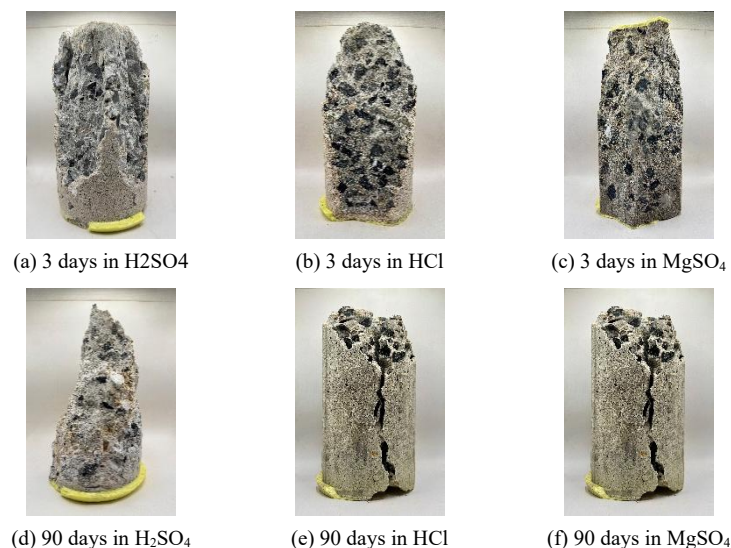
Figure 12. Failure mode of specimens under 20% concentration exposure

For pre-compressive test, submerged H2SO4 immersion specimens, crack lines on the specimen surface were recognizable at early age of immersion. For 60-90days immersion, the surface of specimens was severely damaged. Aggregates disintegrated from the matrix. Especially at 90days immersion, the matrix of specimen was transformed from hardened into soft mud-like with light grey color. The longer immersion duration, the lesser the crack length on the surface. This was mainly due to the specimens with long period of immersion had a relative poor matrix bonding strength and high porosity. For post compressive test specimens, the specimens submerged for 3-28days, the ends of specimens were fully damaged by acidic solution. Crack lines occurred at the middle section of specimen and grew diagonally toward ends. This was due to high stress concentrations at the edges of the load application area. The development of inclined cracks that propagate at an angle to the applied load, leading to a shear plane. The loss of bonding strength increased with chemical concentration and immersion period increased. However, the surface deterioration and crack formation were reduced when chemical concentration increased. For 60-90days immersion, specimens collapsed as compressive stress was applied on the specimens. The deterioration of the specimens was caused by the formation of expansive ettrigite and gypsum due to sulfuric acid. The texture of matrix was softening which led Ca2+ in the matrix decreased. Thus, compressive strength decreased. The two failure patterns were mostly found in residual specimens submerged in H2SO4 solution: cone with split pattern and cone with shear pattern. The failure mode shifted from cone with split pattern to cone with shear pattern when chemical concentration and immersion duration increased.

For HCl, the observation was taken on pre-compressive test specimens, crack lines were confined to the surface of the specimens. For 60-90 days immersion, the crack lines were obviously recognized. The width of crack lines was approximately 1-1.3 mm. Post-compressive test, the ends and middle section of specimens were fully exploded. The crack lines were non-linear with diagonal crack patterns. At 90 days of immersion in 20% concentration, the central crack lines widened, causing specimens to split into two halves. The axial splitting can be seen in short period of immersion and high concentration or long period of immersion with low concentration condition. The width of crack was 3-4 mm. Instead of one main line crack, several crack lines were initiated, a sudden drop in compressive strength when compressive load was increased. Crack propagated vertically and several crack line branches occurred. The normal shear failure mode was mainly failure pattern found in the specimens. However, the columnar failure pattern became more obvious when chemical concentration and immersion duration increased. A well-formed cone was present on one end, while vertical cracks running through the cap with no well-defined cone on the other end.

For MgSO4, pre-compressive test, specimens showed noticeable swelling, with crack initiation from interior toward the surface. The efflorescence was noticed in localized areas. For 60-90 days immersion, the crack width was approximately 3-4 mm. Post-compressive test, the upper end of specimen were mainly exploded when specimens were submerged in chemical solution for 60 days. The crack pattern was recognized as cone failure pattern. The crack width continued to enlarge when specimens were further kept in chemical solution. The crack width was approximately 5-6 mm. However, the failure mode shifted from cone failure pattern to columnar mode pattern and shear as concentration of solution and immersion duration increased.

3.3.2. Splitting Tensile Strength

Figures 13-a to 13-c compared the splitting tensile strength of prepared porcelain-based geopolymer concrete. Cylindrical specimens were prepared using the optimum results. When subjected to H$_2$SO$_4$ solution, specimens experienced a decrease in strength with increasing solution concentrations. Figures 13-a and 13-b showed the acid

resistance of porcelain-based geopolymer concrete specimens in terms of residual strength after exposure to 5%, 10%, 15%, and 20% H_2SO_4 solutions. The deterioration of the specimens was evident as a decrease in residual strength. After 7-days in 5% and 10% H_2SO_4 solutions, the splitting strengths were 2.96 N/mm² and 2.79 N/mm² respectively. After 28-days of immersion, the strength gradually decreased to 2.13 N/mm² and 1.89 N/mm² respectively. The primary factor contributing to the strength reduction in porcelain-based geopolymer concrete was the degradation of aluminosilicate bonds within the matrix. This weakened both internal and external structures, leading to a decline in overall strength. The highest decrease in splitting strength was found in specimens immersed for 90-days which was caused by acid corrosion. The residual strength remained only 0.40 N/mm². The rate of decrease in strength was most pronounced during the 21-days of immersion. A similar pattern was found in compressive strength results. At the early ages of immersion, the rate of deterioration decreased after 7-days before gradually increasing towards 21-days of immersion. The rate of deterioration then declined again towards the 90-days immersion period. It was found that the level of solution concentration affected the rate of deterioration in strength. The relationship between the weight change due to sulfuric acid attack on concretes and the immersion time was shown in Table 4. For porcelain-based concrete, weight losses were primarily due to the reaction between calcium hydroxide present in the specimens and the acid, which induced tensile stress, resulting in the formation of cracking and scaling. The highest loss in weight occurred during the first 7-days of immersion. The rate of weight loss was 31.23% per day for the 20% H_2SO_4 solution. The rate of weight loss decreased over time, possibly due to the solution becoming saturated. The calcium released from specimens was due to H_2SO_4 corrosion. Additionally, porcelain contained low calcium content. The amount of calcium used in the geopolymerization process was limited compared to high-calcium binder materials. The internal structure of the geopolymer was more susceptible to deterioration. Similar results were found by Thokchom et al. [57] and Sata et al. [37].
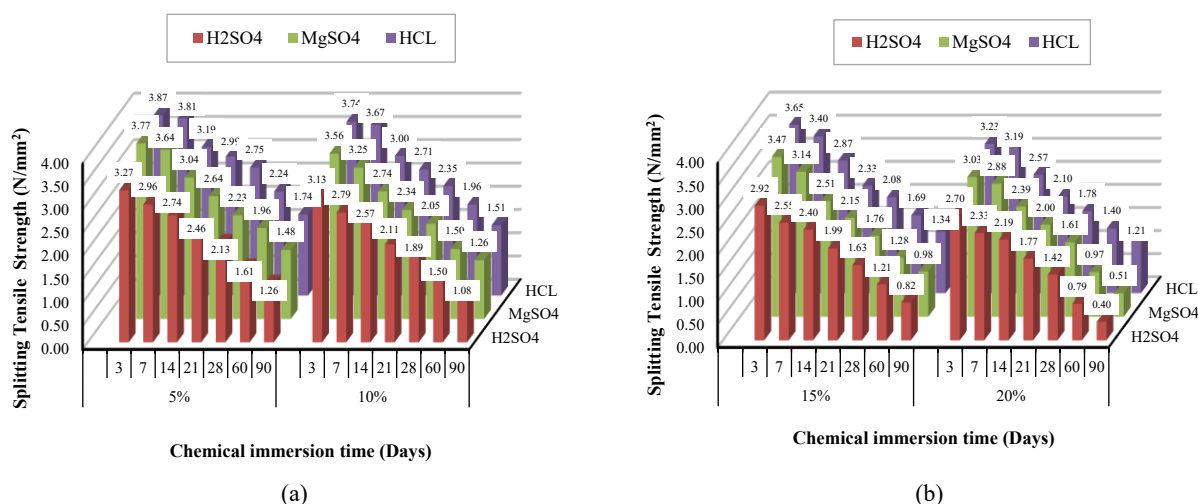
Figure 13. Residual splitting tensile strength of specimens

In HCl condition, it appeared that the specimens exposed to HCl had a higher residual strength than the specimens exposed to H_2SO_4 solution. A similar result was found in fly ash type F with sodium and potassium activators. This might be due to the expansion caused by sulfate species as H_2SO_4 had a more deteriorating effect on the microstructure than HCl. The level of deterioration caused by H_2SO_4 might have induced SO_4^{2-} ion migration. Figure 13-a showed the deterioration of specimens. It was found that the weight loss of the specimens exposed to 5% and 10% HCl solutions was 19.14%, 3.21%, 12.39%, 4.92%, 3.07%, 1.97% and 19.21%, 4.52%, 12.75%, 7.43%, 3.29%, 2.46% per day respectively. Specimens submerged in sulfuric acid exhibited greater deterioration, characterized by scaling and mineral leaching from the aluminosilicate gel. In contrast, specimens exposed to HCl solution experienced deterioration primarily through leaching, which was marked by decolorization [43, 56, 58-61]. At an early age of immersion, the rate of weight loss rapidly increased. At 7-days of immersion, the weight of specimens reduced at a rate of 22.06% per day for 20% HCl concentration (Table 4). The rate then gradually declined towards the end of the experiment. It appeared that the concentration of the HCl solution affected the rate of weight loss of porcelain-based geopolymer concrete. The higher the HCl concentration of the solution applied to specimens, the faster the rate of weight loss became.

For $MgSO_4$, the splitting strength decreased with increasing immersion time. The splitting tensile strength results were compared at an immersion time of 14 days. The reduction rate of splitting tensile strength for 5%, 10%, 15%, and 20% concentrations of $MgSO_4$ solution was 3.04, 2.74, 2.51 and 2.39 N/mm² per day respectively. A loss of strength after exposure to an $MgSO_4$ solution was also found by Bakharev [9]. This was due to alkalis migrating into the solution. Meanwhile, the change in weight rapidly increased during the 14-days of immersion. The increment in weight for 5%, 10%, 15%, and 20% concentrations was +13.81, +6.22, +3.69, +1.20, +1.58 and +0.64% per day respectively.

Table 4. The reduction rate of splitting tensile strength and changing in weight of specimens

Type of chemical immersion	Reduction rate of splitting tensile strength (N/mm² per day)						Change in weight (% per day)					
	3⇒7 days	7⇒14 days	14⇒21 days	21⇒28 days	28⇒60 days	60⇒90 days	3⇒7 days	7⇒14 days	14⇒21 days	21⇒28 days	28⇒60 days	60⇒90 days
5%H₂SO₄	0.08	0.03	0.04	0.05	0.02	0.01	-23.77	-7.09	-12.63	-9.40	-3.66	-2.03
5%HCl	0.02	0.09	0.03	0.04	0.02	0.01	-19.14	-3.21	-12.39	-4.92	-3.07	-1.97
5%MgSO₄	0.03	0.09	0.05	0.60	0.01	0.01	+13.81	+6.22	+3.69	+1.20	+1.58	+0.64
10%H₂SO₄	0.08	0.03	0.06	0.03	0.02	0.01	-27.22	-13.29	-6.41	-11.41	-3.70	-2.95
10%HCl	0.02	0.09	0.04	0.05	0.02	0.01	-19.21	-4.52	-12.75	-7.43	-3.29	-2.46
10%MgSO₄	0.08	0.07	0.65	0.04	0.02	0.01	+15.82	+6.50	+2.86	+3.13	+1.03	+0.17
15%H₂SO₄	0.09	0.02	0.06	0.05	0.02	0.01	-29.15	-14.58	-5.39	-12.58	-3.69	-2.43
15%HCl	0.06	0.08	0.08	0.04	0.02	0.01	-20.29	-7.53	-13.39	-10.22	-3.51	-2.58
15%MgSO₄	0.08	0.09	0.05	0.06	0.02	0.01	+18.03	+13.60	+3.49	+3.89	+0.19	+0.41
20%H₂SO₄	0.09	0.02	0.06	0.05	0.021	0.01	-31.23	-14.45	-31.68	-14.85	-2.95	-1.56
20%HCl	0.05	0.08	0.07	0.04	0.02	0.01	-22.06	-7.74	-14.03	-11.04	-3.73	-2.63
20%MgSO₄	0.04	0.72	0.06	0.05	0.02	0.01	+18.30	+14.43	+4.84	+5.08	+0.41	+0.16

The specimens exposed to 15% and 20% MgSO₄ solution, the average 28-days and 90-days splitting tensile strength dropped to 1.76 N/mm², 1.61 N/mm² and 1.08 N/mm², 0.63 N/mm² respectively. This indicated that the MgSO₄ solution continued to disrupt the aluminosilicate structure, resulting in structural deterioration. It also suggests that porcelain and fly ash Type F binder materials exhibit weak Si-rich (C-A-S-H gel) desilication [62]. Deterioration caused by MgSO₄ exposure was primarily due to calcium leaching. Sulfate corrosion expanded the pores, accelerating the movment of deteriorated and leached components into the matrix. The porcelain-based geopolymer concrete specimens exhibited increased degradation in sulfated solution. This degradation was marked by strength loss and the formation of precipitated salts on the surface. The extent of salt deposition intensified with prolonged immersion and higher solution concentrations.

However, fluctuations in weight gain were observed due to the lower silica-to-alumina ratio. Consequently, the low calcium content contributed to an unstable geopolymerization process, affecting the rate of changing weight. A similar result was found by Jiao et al. [63]. Upon exposure to MgSO₄ solution, the weight change of the specimens was smaller than that of the geopolymer concrete immersed in H₂SO₄ and HCl. The opposite trend was noticed for the specimens in MgSO₄ immersion. The specimen weight increased due to precipitation products. All specimens continued to experience weight increment. This might be due to regular maintenance of the pH and solution concentration through replenishment, which also contributed to alkali leaching from the specimens [64]. It was observed that all specimens retained partial strength in failure mode when submerged for over 28 days. These results align with the strength reduction rate, which eventually diminished to zero. The strength of the gel was weakened by sulfuric acid and sulfate attack.

3.3.3. Relationship Between Residual of Compressive and Splitting Tensile Strength

In order to understand the statistical relationship between splitting tensile strengths and compressive strength of porcelain based geopolymer concrete were established in Figures 14-a to 14-c under chemical corrosion environment. An empirical formula between splitting tensile strength (f_{sp}) and compressive strength (f_c) proposed by various researchers, was used as showed in Equation 3.

$$f_{sp} = x(f_c)^n \tag{3}$$

where f_c was compressive strength n and x were constant coefficients.

In addition to those specimens were subjected to compressive test, the cylindrical specimens were also subjected to splitting tensile strength test. It was noticed from Table 5 that the splitting tensile strength (f_{sp}) of porcelain based geopolymer concrete had relationship to compressive strength results where the higher the specimen strength, the greater the splitting tensile strength. The higher compressive strength usually corresponded to its higher splitting tensile strength. The ratio of splitting tensile and compressive strength decreased with immersion duration. The ratio of f_{sp}/f'_c varied in the range of 0.077 to 0.167. Similar result was found in geopolymer concrete mixed with fly ash Type F under normal condition [65]. The constant coefficient (x) were ranged between 0.23 to 0.59. The deterioration rate of submerged specimens in acidic and alkaline environments had a minimal effect on the ratio of splitting tensile strength to compressive strength. The constant coefficient (n) of relationship between splitting tensile strength and compressive strength also decreased with the immersion duration.
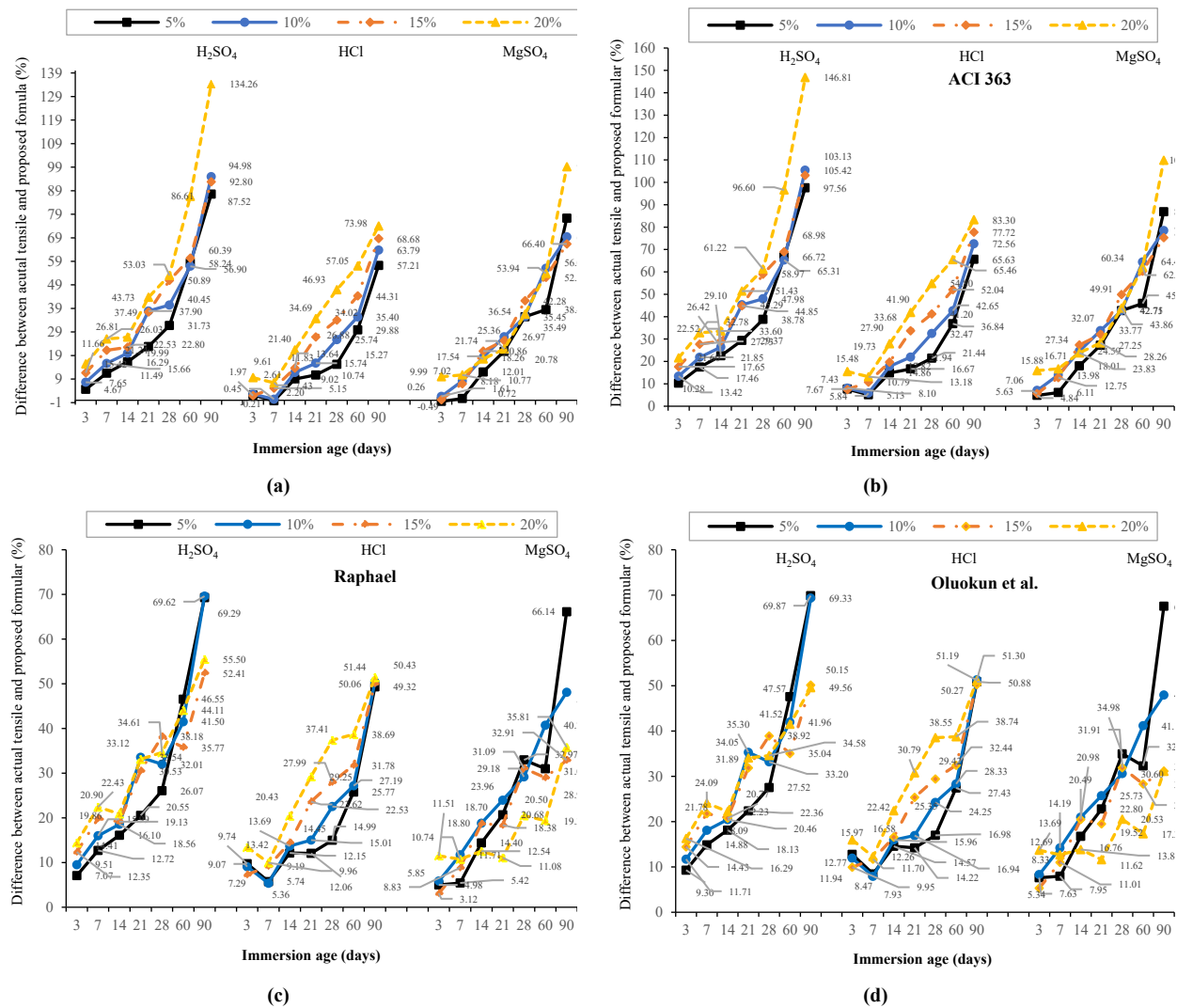
Figure 14. Difference in percentage of splitting tensile compared with others

Table 5. Compared empirical relationships between compressive strength (f_c) and splitting tensile strength (f_sp)

Type of Chemical Immersion	Predicted splitting tensile strength by using others proposed formula (N/mm²)					Difference in percentage of strengths (residual strength compared with others under normal environment (%))				
	ACI 318 [66]	ACI 363 [67]	Raphael [68]	Oluokun et al. [69]	Arıoglu et al. [70]	$Difference\ in\ tensile\ (\%) = \left(\frac{f_{cr\,(results)} - f_{cr\,(proposed\,by\,others)}}{f_{cr\,(proposed\,by\,others)}}\right) \times 100$ where; $x = \frac{f_{cr}}{\sqrt{f_c}}$				
	Normal concrete	High strength	Normal weight	Early age concrete	Geopolymer fly-ash type C	ACI 318 [66]	ACI 363 [67]	Raphael [68]	Oluokun et al. [69]	Arıoglu et al. [70]
	$f_{cr} = 0.56\sqrt{f_c}$	$f_{cr} = 0.59\sqrt{f_c}$	$f_{cr} = 0.313 f_c^{0.667}$	$f_{cr} = 0.294 f_c^{0.69}$	$f_{cr} = 0.249 f_c^{0.772}$					
	28 days	28 days	28 days	7 days	7 days	28 days	28 days	28 days	7 days	7 days
5%H₂SO₄	2.802	2.952	2.682	3.403	3.856	31.72	38.78	26.07	14.88	30.16
5%HCl	3.172	3.342	3.165	4.132	4.791	15.26	21.44	14.98	8.47	25.77
5%MgSO₃	3.024	3.186	2.968	3.926	4.525	35.45	42.70	32.97	7.95	24.44
10%H₂SO₄	2.654	2.796	2.494	3.291	3.714	40.45	47.97	32.00	18.08	33.26
10%HCl	2.957	3.116	2.882	3.960	3.955	25.73	32.47	22.52	7.92	24.51
10%MgSO₄	2.770	2.919	2.641	3.714	4.252	35.48	42.74	29.17	14.19	30.73
15%H₂SO₄	2.455	2.587	2.248	3.102	3.476	50.88	58.97	38.17	21.78	36.47
15%HCl	2.784	2.933	2.659	3.800	4.363	34.02	41.20	27.98	11.69	28.23
15%MgSO₄	2.500	2.634	2.303	3.486	4.173	42.28	49.90	31.08	11.00	26.13
20%H₂SO₄	2.176	2.293	1.914	2.885	3.205	53.02	61.22	34.60	24.09	37.87
20%HCl	2.615	2.755	2.445	3.581	4.082	46.92	54.79	37.40	12.26	27.97
20%MgSO₄	2.198	2.316	1.940	3.248	3.659	36.54	43.85	20.49	12.68	26.97

The splitting tensile strength obtained from the experiments had similar results to those design codes and several empirical equations when early age of specimen values were compared [66]. For 3-days and 7-days H_2SO_4 immersion, the difference between the splitting tensile experimental values and ACI 318 values at 5% and 10% concentration were 4.67%, 7.65% and 11.48%, 15.65% respectively. The difference in experimental values and proposed formula values by others increased toward the end of experiment [67-70]. This might due to deterioration of specimen under acidic and alkaline environment which caused the formation of cracks and spalling. In this study, the experimental data also fell below the others' proposed formula values. Table 5 showed comparative empirical relationship between compressive and splitting tensile strength. A similar result was also found in geopolymer concrete mixed with fly ash type F by Gartner [71]. The ACI 318 and ACI 363 relationships for compressive strength and splitting tensile strength were shown to be conservative. The normal concrete tensile strength prediction formula, predicted above experimental values. Three additional formulas of this relationship were also plotted where the constant coefficient (*x*) were 0.59, 0.313 and 0.294 for high strength concrete, normal weight concrete and early age concrete respectively. While, *n* was governed at 0.5 [61], 0.667 [72] and 0.69 [73] respectively. It found that the relationship between splitting tensile strength and compressive strength of porcelain based geopolymer concrete was similar to the Ordinary Portland Cement concrete. It appeared that the ACI-318-99 was suited for geopolymer concrete splitting tensile strength prediction where specimens was submerged in solution for 3-7 days [74]. However, 28-days, 60-days and 90-days aged concrete were individually considered. After 28 days, the new relationship model was required for geopolymer concrete based low calcium binder material. The ratio of the two strengths (f_{sp}/f'_c) was strongly affected by the increment of the compressive strength. The ratio decreased with increasing compressive strength at a decreasing rate. This indicated that an increment rate of splitting tensile strength was lower than an increment rate of compressive strength. At early age, 5% H_2SO_4 concentration solution, the splitting tensile strengths were as high as 8.7% of the cylinder compressive strength whereas at 90-days immersion duration, the ratio reduced to approximately 7.1%.

For HCl, the cylinder specimens that were exposed to 5% and 10% concentration solution exposures. The splitting tensile strength to compressive strength ratio for 7-days and 14-days immersion was 0.083, 0.082 and 0.084, 0.083 respectively. The ratios decreased toward 90-days of immersion. The rate decrease was lower than H_2SO_4, while the constant coefficient (*n*) was higher than those in H_2SO_4. The increment in n values were 12% and 6.5% respectively when compared with H_2SO_4. The percentage difference between experimental values and proposed formula values at 7-days and 14-days immersion for 5%, 10%, 15% and 20% concentration solution was 5.13%, 5.83%, 10.78% and 13.18% respectively. It also found that nonlinear relationship between experimental results and predicted splitting tensile strength from all relations showed in Figure 14-a to 14-d. The difference between the splitting tensile of experimental value and proposed value at 3-days immersion for 5% and 10% concentration of solution was compared, the actual value was underestimate by 2.19% and 2.60% respectively. As the period of immersion and the level of concentration of solution increased, the difference in values rapidly increased. At 90-days immersion, the difference between actual and proposed values were 57.21% and 63.79% respectively.

In $MgSO_4$ environment, the average splitting tensile strength and compressive strength ratio at 7-days and 14-days immersion results were showed in Table 6. It found that the porcelain based geopolymer concrete gave lower tensile when compared with HCl. The higher concentration of solution resulted in a lower splitting tensile strength to compressive strength ratio. Similar results were found in H_2SO_4 and HCl.

Table 5. Ratio of compressive and splitting tensile strength and constant coefficient factor (n)

Type of chemical immersion	Ratio of splitting and compressive $= \frac{f_{sp}}{f'_c}$							$x = \frac{f_{sp}}{\sqrt{f'_c}}$						
	3 days	7 days	14 days	21 days	28 days	60 days	90 days	3 days	7 days	14 days	21 days	28 days	60 days	90 days
5%H_2SO_4	0.087	0.085	0.085	0.084	0.085	0.078	0.071	0.53	0.50	0.48	0.46	0.43	0.35	0.30
5%HCl	0.077	0.083	0.082	0.085	0.085	0.083	0.073	0.55	0.56	0.51	0.50	0.49	0.43	0.36
5%$MgSO_4$	0.084	0.085	0.082	0.081	0.076	0.083	0.067	0.56	0.56	0.49	0.46	0.41	0.40	0.32
10%H_2SO_4	0.086	0.084	0.084	0.078	0.084	0.085	0.076	0.52	0.48	0.47	0.41	0.40	0.36	0.29
10%HCl	0.079	0.084	0.083	0.086	0.086	0.087	0.077	0.59	0.56	0.50	0.48	0.44	0.41	0.34
10%$MgSO_4$	0.089	0.087	0.086	0.093	0.088	0.105	0.116	0.56	0.52	0.47	0.44	0.40	0.36	0.33
15%H_2SO_4	0.086	0.083	0.085	0.085	0.082	0.088	0.080	0.50	0.46	0.45	0.41	0.37	0.35	0.30
15%HCl	0.083	0.083	0.085	0.083	0.084	0.089	0.082	0.55	0.53	0.49	0.44	0.42	0.39	0.33
15%$MgSO_4$	0.089	0.087	0.086	0.093	0.089	0.113	0.127	0.56	0.52	0.46	0.45	0.39	0.36	0.34
20%H_2SO_4	0.087	0.084	0.089	0.086	0.094	0.156	0.167	0.51	0.50	0.47	0.46	0.41	0.36	0.28
20%HCl	0.080	0.085	0.082	0.083	0.082	0.091	0.083	0.48	0.44	0.44	0.38	0.38	0.36	0.23
20%$MgSO_4$	0.087	0.085	0.089	0.858	0.094	0.113	0.142	0.51	0.51	0.48	0.46	0.41	0.43	0.34

At 3-days immersion, the difference between the splitting tensile experimental and predicted values (ACI 318) for 5% and 10% concentration of solution was overestimate by 0.48% and underestimate by 1.61% respectively (Table 6). Comparatively, 60-days and 90-days immersion, the difference between experimental value and predicted values were 45.89%, 86.83% and 64.41% and 78.44% respectively. The accuracy of relationship was very low when immersion duration increased. It appeared among ACI 318, ACI 363, Raphael and Oluokun proposed formulas (Figures 14-a to 14-d) that the ACI 318 provided a suitable fit only for early age prediction values when specimens were submerged in acidic and alkaline environments. However, the errors in previously proposed formulas increased, with significant variability remaining. This occurred because magnesium salt weakened the specimens as its concentration rose, causing a rapid decrease in strength [70]. In addition, the anions of sulfate were also ingress into geopolymer specimens. While, the precipitation of alkali was caused by magnesium cation reduced both the alkalinity and strength of specimens. In view of the numerous factors influencing the relationship of the strength of concrete, it was expected that there was no simple exact relation was applicable. The correlations were felt to be representative in lieu of specific testing for concrete design and evaluation.

4. Conclusion

This study presented an experimental investigation the effect of acidic and alkaline corrosion on porcelain-based geopolymer concrete under compressive loading. An analytical study was carried out on the compressive strength and splitting tensile strength over 3, 7, 14, 21, 28, 60 and 90-days corresponding to porcelain-based geopolymer concrete with 14M and an initial curing temperature of 105°C for 24 hours. Based on the results, the following conclusions were made:

The analysis of the microstructure of porcelain-based geopolymer concrete using SEM showed a good reaction to the constituent materials of the specimen. The results of XRD analysis on a 20% concentration solution for 60-days immersion showed that submerged specimens in H_2SO_4 mainly consisted of SiO_2, gypsum, and graphite, while those submerged in HCl comprised $CaCO_3$, SiO_2, and mullite. The submerged specimens in $MgSO_4$ were largely composed of SiO_2, mullite, $CaCO_3$ and merwinite. The peak was at an angle position of $2\theta = 26.8$.

The immersion of specimens in H_2SO_4, HCl, and $MgSO_4$ solutions with concentrations of 5%, 10%, 15%, and 20% affected the weight loss, compressive strength and splitting tensile strength. After immersion, the weight and strengths of specimens decreased with an increment of solution concentration and immersion period. The residual compressive strength of porcelain-based geopolymer specimens after exposure to 5%, 10%, 15%, and 20% H_2SO_4, HCl, and $MgSO_4$ separately showed that the deterioration of specimens exposed to H_2SO_4 was the highest compared to those exposed to HCl and $MgSO_4$. The ability to resist degradation and corrosion of sodium-activated porcelain-based geopolymer concretes was acceptable. The maximum residual compressive strengths of 37.30 N/mm², 49.88 N/mm², and 44.88 N/mm² were found in 5% incorporated porcelain-based geopolymer concrete exposed to H_2SO_4, HCl, and $MgSO_4$ for 3 days immersion, respectively. The failure pattern of specimens submerged in H_2SO_4 shifted from a cone with a split pattern to a cone with shear pattern. For HCl, the normal shear failure mode transitioned to a columnar failure pattern. In the case of $MgSO_4$, the failure mode changed from a cone failure pattern to a combination of columnar and shear mode as chemical concentration and immersion duration increased.

The porcelain-based geopolymer concrete displayed splitting tensile strength ranging from 0.40 N/mm² to 3.87 N/mm² when exposed to 5% and 20% of H_2SO_4 and HCl solutions, respectively. Among submerged specimens, those submerged in HCl solution showed moderate deterioration, with maximum residual splitting tensile strength at 3.87 N/mm² after exposure to 5% HCl solution for 3-days immersion. Magnesium sulfate induced the transformation of low-calcium hydrate gels within the matrix, resulting in deterioration. The strength degradation of porcelain-based geopolymer was governed by the concentration of solutions and the immersion period. The highest rate of degradation from H_2SO_4 occurred during the 3-7 days immersion period, while for HCl and $MgSO_4$, it occurred during the 7-14 days immersion period. The splitting tensile strength of concrete increased with compressive strength, and the splitting tensile strength to compressive strength (f_{sp}/f'_c) ratio decreased as the compressive strength increased. The splitting tensile strength obtained from experimental data was closely aligned with the ACI 318 design code when compared based on the experimental data. The ratio of f_{sp}/f'_c varied between 0.077 and 0.167. The splitting tensile strength to compressive strength (f_{sp}/f'_c) ratio was influenced by the level of solution concentration and the immersion period. At early stage of immersion, the splitting tensile strengths were as high as 8.9% of the cylinder compressive strength. At 90-days immersion, The ratio of f_{sp}/f'_c reduced to approximately 6.7%. The 0.5 power relationship between splitting tensile strength and cylinder compressive strength was found to be unrealistic. While the ACI-318 model overestimated the strength of porcelain-based geopolymer concrete, it was closer to experimental values compared to the ACI 363 model.

5. Declarations

5.1. Author Contributions

5.2. Data Availability Statement

The data presented in this study are available on request from the corresponding author.

5.3. Funding

5.4. Acknowledgements

5.5. Conflicts of Interest

The authors declare no conflict of interest.

6. References

[1] Desole, M. P., Fedele, L., Gisario, A., & Barletta, M. (2024). Life Cycle Assessment (LCA) of ceramic sanitaryware: focus on the production process and analysis of scenario. International Journal of Environmental Science and Technology, 21(2), 1649–1670. doi:10.1007/s13762-023-05074-6.

[2] Cuviella-Suárez, C., Borge-Diez, D., & Colmenar-Santos, A. (2021). Introduction to Ceramic Sanitary-Ware Manufacturing. Water and Energy Use in Sanitary-ware Manufacturing. Green Energy and Technology. Springer, Cham, Switzerland. doi:10.1007/978-3-030-72491-7_1.

[3] Furszyfer Del Rio, D. D., Sovacool, B. K., Foley, A. M., Griffiths, S., Bazilian, M., Kim, J., & Rooney, D. (2022). Decarbonizing the ceramics industry: A systematic and critical review of policy options, developments and sociotechnical systems. Renewable and Sustainable Energy Reviews, 157. doi:10.1016/j.rser.2022.112081.

[4] Santos, T., Almeida, J., Silvestre, J. D., & Faria, P. (2021). Life cycle assessment of mortars: A review on technical potential and drawbacks. Construction and Building Materials, 288. doi:10.1016/j.conbuildmat.2021.123069.

[5] Pitarch, A. M., Reig, L., Tomás, A. E., Forcada, G., Soriano, L., Borrachero, M. V., Payá, J., & Monzó, J. M. (2021). Pozzolanic activity of tiles, bricks and ceramic sanitary-ware in eco-friendly Portland blended cements. Journal of Cleaner Production, 279, 123713. doi:10.1016/j.jclepro.2020.123713.

[6] Bernasconi, A., Pellegrino, L., Vergani, F., Campanale, F., Marian, N. M., Galimberti, L., Perotti, M., Viti, C., & Capitani, G. (2023). Recycling detoxified cement asbestos slates in the production of ceramic sanitary wares. Ceramics International, 49(2), 1836–1845. doi:10.1016/j.ceramint.2022.09.147.

[7] Farinha, C. B., Silvestre, J. D., de Brito, J., & Veiga, M. do R. (2019). Life cycle assessment of mortars with incorporation of industrial wastes. Fibers, 7(7), 59. doi:10.3390/FIB7070059.

[8] Pather, B., Ekolu, S. O., & Quainoo, H. (2021). Effects of aggregate types on acid corrosion attack upon fly–Ash geopolymer and Portland cement concretes–Comparative study. Construction and Building Materials, 313, 125468. doi:10.1016/j.conbuildmat.2021.125468.

[9] Bakharev, T. (2005). Durability of geopolymer materials in sodium and magnesium sulfate solutions. Cement and Concrete Research, 35(6), 1233–1246. doi:10.1016/j.cemconres.2004.09.002.

[10] Noushini, A., Castel, A., Aldred, J., & Rawal, A. (2020). Chloride diffusion resistance and chloride binding capacity of fly ash-based geopolymer concrete. Cement and Concrete Composites, 105. doi:10.1016/j.cemconcomp.2019.04.006.

[11] Kaplan, G., Yavuz Bayraktar, O., Bayrak, B., Celebi, O., Bodur, B., Oz, A., & Aydin, A. C. (2023). Physico-mechanical, thermal insulation and resistance characteristics of diatomite and attapulgite based geopolymer foam concrete: Effect of different curing regimes. Construction and Building Materials, 373. doi:10.1016/j.conbuildmat.2023.130850.

[12] Liu, M. Y. J., Alengaram, U. J., Jumaat, M. Z., & Mo, K. H. (2014). Evaluation of thermal conductivity, mechanical and transport properties of lightweight aggregate foamed geopolymer concrete. Energy and Buildings, 72, 238–245. doi:10.1016/j.enbuild.2013.12.029.

[13] Eisa, M. S., Basiouny, M. E., & Fahmy, E. A. (2022). Drying shrinkage and thermal expansion of metakaolin-based geopolymer concrete pavement reinforced with biaxial geogrid. Case Studies in Construction Materials, 17, 1415. doi:10.1016/j.cscm.2022.e01415.

[14] Miranda, J. M., Fernández-Jiménez, A., González, J. A., & Palomo, A. (2005). Corrosion resistance in activated fly ash mortars. Cement and Concrete Research, 35(6), 1210–1217. doi:10.1016/j.cemconres.2004.07.030.

[15] Kupwade-Patil, K., & Allouche, E. N. (2013). Examination of Chloride-Induced Corrosion in Reinforced Geopolymer Concretes. Journal of Materials in Civil Engineering, 25(10), 1465–1476. doi:10.1061/(asce)mt.1943-5533.0000672.

[16] Chindaprasirt, P., & Chalee, W. (2014). Effect of sodium hydroxide concentration on chloride penetration and steel corrosion of fly ash-based geopolymer concrete under marine site. Construction and Building Materials, 63, 303–310. doi:10.1016/j.conbuildmat.2014.04.010.

[17] Noushini, A., & Castel, A. (2016). The effect of heat-curing on transport properties of low-calcium fly ash-based geopolymer concrete. Construction and Building Materials, 112, 464–477. doi:10.1016/j.conbuildmat.2016.02.210.

[18] Reddy, D. V., Edouard, J.-B., & Sobhan, K. (2013). Durability of Fly Ash–Based Geopolymer Structural Concrete in the Marine Environment. Journal of Materials in Civil Engineering, 25(6), 781–787. doi:10.1061/(asce)mt.1943-5533.0000632.

[19] Olivia, M., & Nikraz, H. (2012). Properties of fly ash geopolymer concrete designed by Taguchi method. Materials and Design, 36, 191–198. doi:10.1016/j.matdes.2011.10.036.

[20] Geraldo, R. H., Fernandes, L. F. R., & Camarini, G. (2021). Mechanical properties of porcelain waste alkali-activated mortar. Open Ceramics, 8, 100184. doi:10.1016/j.oceram.2021.100184.

[21] Aldawsari, S., & Kampmann, R. (2025). Durability of fly ash/slag geopolymers: Role of OPC and silica under sulfate attack. Construction and Building Materials, 465, 139855. doi:10.1016/j.conbuildmat.2025.139855.

[22] Singh, R. P., Vanapalli, K. R., Jadda, K., & Mohanty, B. (2024). Durability assessment of fly ash, GGBS, and silica fume based geopolymer concrete with recycled aggregates against acid and sulfate attack. Journal of Building Engineering, 82, 108354. doi:10.1016/j.jobe.2023.108354.

[23] Bai, Y., Guo, W., Zhao, Q., Zhang, N., Xue, C., Wang, S., & Song, Y. (2023). Performance deterioration of municipal solid waste incineration fly ash-based geopolymer under sulfuric acid attack. Construction and Building Materials, 391, 131847. doi:10.1016/j.conbuildmat.2023.131847.

[24] Berkouche, A., Belkadi, A. A., Benaddache, L., Tayebi, T., & Aggoun, S. (2025). Enhancing physical, mechanical, and durability properties of slag-based geopolymers through ceramic waste incorporation: A comprehensive optimization study. Journal of the Taiwan Institute of Chemical Engineers, 172, 106144. doi:10.1016/j.jtice.2025.106144.

[25] Abdelmonem, A. M., Azam, A., Alruwaili, A., Ouda, A. S., & Elrahman, M. A. (2025). Effect of ceramic tile waste addition on the performance of slag-based geopolymer upon exposure to marine conditions: Physico-mechanical characteristics, and shielding proficiency against ionizing radiation. Sustainable Chemistry and Pharmacy, 43, 101886. doi:10.1016/j.scp.2024.101886.

[26] Mohebi, R., Behfarnia, K., & Shojaei, M. (2015). Abrasion resistance of alkali-activated slag concrete designed by Taguchi method. Construction and Building Materials, 98, 792–798. doi:10.1016/j.conbuildmat.2015.08.128.

[27] Yan, B., Duan, P., & Ren, D. (2017). Mechanical strength, surface abrasion resistance and microstructure of fly ash-metakaolin-sepiolite geopolymer composites. Ceramics International, 43(1), 1052–1060. doi:10.1016/j.ceramint.2016.10.039.

[28] Luhar, S., Chaudhary, S., & Luhar, I. (2019). Development of rubberized geopolymer concrete: Strength and durability studies. Construction and Building Materials, 204, 740–753. doi:10.1016/j.conbuildmat.2019.01.185.

[29] Witzke, F. B., Beltrame, N. A. M., Angulski da Luz, C., & Medeiros-Junior, R. A. (2023). Abrasion resistance of metakaolin-based geopolymers through accelerated testing and natural wear. Wear, 530–531. doi:10.1016/j.wear.2023.204996.

[30] Noushini, A., Hastings, M., Castel, A., & Aslani, F. (2018). Mechanical and flexural performance of synthetic fibre reinforced geopolymer concrete. Construction and Building Materials, 186, 454–475. doi:10.1016/j.conbuildmat.2018.07.110.

[31] Arslan, A. A., Uysal, M., Yılmaz, A., Al-mashhadani, M. M., Canpolat, O., Şahin, F., & Aygörmez, Y. (2019). Influence of wetting-drying curing system on the performance of fiber reinforced metakaolin-based geopolymer composites. Construction and Building Materials, 225, 909–926. doi:10.1016/j.conbuildmat.2019.07.235.

[32] ASTM C496/C496M-11. (2017). Standard Test Method for Splitting Tensile Strength of Cylindrical Concrete Specimens. ASTM International, Pennsylvania, United States. doi:10.1520/C0496_C0496M-11.

[33] ASTM C39/C39M-99. (2017). Standard Test Method for Compressive Strength of Cylindrical Concrete Specimens. ASTM International, Pennsylvania, United States. doi:10.1520/C0039_C0039M-99.

[34] Yang, W., Zhu, P., Liu, H., Wang, X., Ge, W., & Hua, M. (2021). Resistance to sulfuric acid corrosion of geopolymer concrete based on different binding materials and Alkali concentrations. Materials, 14(23), 7109. doi:10.3390/ma14237109.

[35] Aiken, T. A., Kwasny, J., Sha, W., & Soutsos, M. N. (2018). Effect of slag content and activator dosage on the resistance of fly ash geopolymer binders to sulfuric acid attack. Cement and Concrete Research, 111, 23–40. doi:10.1016/j.cemconres.2018.06.011.

[36] Patrisia, Y., Law, D. W., Gunasekara, C., & Wardhono, A. (2022). Fly ash geopolymer concrete durability to sulphate, acid and peat attack. MATEC Web of Conferences, 364, 02003. doi:10.1051/matecconf/202236402003.

[37] Sata, V., Sathonsaowaphak, A., & Chindaprasirt, P. (2012). Resistance of lignite bottom ash geopolymer mortar to sulfate and sulfuric acid attack. Cement and Concrete Composites, 34(5), 700–708. doi:10.1016/j.cemconcomp.2012.01.010.

[38] Izzat, A. M., Al Bakrt, A. M. M., Kamarudin, H., Sandu, A. V., Ruzaidi, G. C. M., Faheem, M. T. M., & Moga, L. M. (2013). Sulfuric acid attack on ordinary Portland cement and geopolymer material. Revista de Chimie, 64(9), 1011–1014.

[39] Zuda, L., Bayer, P., Rovnaník, P., & Černý, R. (2008). Mechanical and hydric properties of alkali-activated aluminosilicate composite with electrical porcelain aggregates. Cement and Concrete Composites, 30(4), 266–273. doi:10.1016/j.cemconcomp.2007.11.003.

[40] Amigó, J. M., Serrano, F. J., Kojdecki, M. A., Bastida, J., Esteve, V., Reventós, M. M., & Martí, F. (2005). X-ray diffraction microstructure analysis of mullite, quartz and corundum in porcelain insulators. Journal of the European Ceramic Society, 25(9), 1479–1486. doi:10.1016/j.jeurceramsoc.2004.05.019.

[41] Valencia-Saavedra, W. G., de Gutiérrez, R. M., & Puertas, F. (2020). Performance of FA-based geopolymer concretes exposed to acetic and sulfuric acids. Construction and Building Materials, 257, 119503. doi:10.1016/j.conbuildmat.2020.119503.

[42] Allahverdi, A., & Skvara, F. (2001). Nitric acid attack on hardened paste of geopolymeric cements, Part 1. Ceramics Silikaty, 45(3), 81-88.

[43] Javed, U., Shaikh, F. U. A., & Sarker, P. K. (2024). Corrosive effect of HCl and H2SO4 exposure on the strength and microstructure of lithium slag geopolymer mortars. Construction and Building Materials, 411, 134588. doi:10.1016/j.conbuildmat.2023.134588.

[44] Kaya, M., Köksal, F., Nodehi, M., Bayram, M., Gencel, O., & Ozbakkaloglu, T. (2022). The Effect of Sodium and Magnesium Sulfate on Physico-Mechanical and Microstructural Properties of Kaolin and Ceramic Powder-Based Geopolymer Mortar. Sustainability (Switzerland), 14(20), 13496. doi:10.3390/su142013496.

[45] Sofi, M., van Deventer, J. S. J., Mendis, P. A., & Lukey, G. C. (2007). Engineering properties of inorganic polymer concretes (IPCs). Cement and Concrete Research, 37(2), 251–257. doi:10.1016/j.cemconres.2006.10.008.

[46] Djwantoro, H., & Rangan, B. V. (2005). Development and properties of low-calcium fly ash-based geopolymer concrete. Research Report GC 1, Curtin University Of Technology, Perth, Australia.

[47] Kränzlein, E., Harmel, J., Pöllmann, H., & Krcmar, W. (2019). Influence of the Si/Al ratio in geopolymers on the stability against acidic attack and the immobilization of Pb2+ and Zn2+. Construction and Building Materials, 227. doi:10.1016/j.conbuildmat.2019.08.015.

[48] Chen, M., Wu, D., Chen, K., Liu, C., Zhou, G., & Cheng, P. (2025). The effects of solid activator dosage and the liquid-solid ratio on the properties of FA-GGBS based one-part geopolymer. Construction and Building Materials, 463. doi:10.1016/j.conbuildmat.2025.140067.

[49] Alzeebaree, R., Çevik, A., Nematollahi, B., Sanjayan, J., Mohammedameen, A., & Gülşan, M. E. (2019). Mechanical properties and durability of unconfined and confined geopolymer concrete with fiber reinforced polymers exposed to sulfuric acid. Construction and Building Materials, 215, 1015–1032. doi:10.1016/j.conbuildmat.2019.04.165.

[50] Temuujin, J., Minjigmaa, A., Lee, M., Chen-Tan, N., & Van Riessen, A. (2011). Characterisation of class F fly ash geopolymer pastes immersed in acid and alkaline solutions. Cement and Concrete Composites, 33(10), 1086–1091. doi:10.1016/j.cemconcomp.2011.08.008.

[51] Rovnaník, P. (2010). Effect of curing temperature on the development of hard structure of metakaolin-based geopolymer. Construction and Building Materials, 24(7), 1176–1183. doi:10.1016/j.conbuildmat.2009.12.023.

[52] Wan-En, O., Yun-Ming, L., Cheng-Yong, H., Abdullah, M. M. A. B., Ngee, H. L., Pakawanit, P., Lee, W. H., Ken, P. W., Hoe-Woon, T., & Yu-Xin, Y. (2024). Magnesium sulphate resistance of fly ash one-part geopolymers: Influence of solid alkali activators on physical, mechanical and chemical performance. Construction and Building Materials, 446, 137971 10 1016 2024 137971. doi:10.1016/j.conbuildmat.2024.137971.

[53] Li, Y., Huang, L., Gao, C., Mao, Z., & Qin, M. (2023). Workability and mechanical properties of GGBS-RFBP-FA ternary composite geopolymer concrete with recycled aggregates containing recycled fireclay brick aggregates. Construction and Building Materials, 392, 131450. doi:10.1016/j.conbuildmat.2023.131450.

[54] Ismail, I., Bernal, S. A., Provis, J. L., Hamdan, S., & Van Deventer, J. S. J. (2013). Microstructural changes in alkali activated fly ash/slag geopolymers with sulfate exposure. Materials and Structures/Materiaux et Constructions, 46(3), 361–373. doi:10.1617/s11527-012-9906-2.

[55] Baščarević, Z., Komljenović, M., Miladinović, Z., Nikolić, V., Marjanović, N., & Petrović, R. (2014). Impact of sodium sulfate solution on mechanical properties and structure of fly ash based geopolymers. Materials and Structures/Materiaux et Constructions, 48(3), 683–697. doi:10.1617/s11527-014-0325-4.

[56] Zhang, B., Huang, D., Li, L., Lin, M., Liu, Y., Fang, W., Lu, J., Liu, F., Li, Y., Liu, Y., & Xiong, Z. (2022). Effect of magnesium salt contamination on the microstructures and properties of metakaolinite-based geopolymer: the role of MgCl2and MgSO4. Journal of Materials Research and Technology, 20, 4500–4514. doi:10.1016/j.jmrt.2022.09.019.

[57] Thokchom, S., Ghosh, P., & Ghosh, S. (2009). Resistance of fly ash based geopolymer mortars in sulfuric acid. ARPN Journal of Engineering and Applied Sciences, 4(1), 65-70.

[58] Al-Jabali, H. M., El-Latief, A. A., Ezz, M. S., Khairy, S., & Nada, A. A. (2024). GGBFS and Red-Mud based Alkali-Activated Concrete Beams: Flexural, Shear and Pull-Out Test Behavior. Civil Engineering Journal, 10(5), 1494–1512. doi:10.28991/CEJ-2024-010-05-09.

[59] Javed, U., Shaikh, F. U. A., & Sarker, P. K. (2022). Microstructural investigation of lithium slag geopolymer pastes containing silica fume and fly ash as additive chemical modifiers. Cement and Concrete Composites, 134, 104736. doi:10.1016/j.cemconcomp.2022.104736.

[60] Intarabut, D., Sukontasukkul, P., Phoo-ngernkham, T., Hanjitsuwan, S., Sata, V., Chumpol, P., … Chindaprasirt, P. (2024). Role of Slag Replacement on Strength Enhancement of One-Part High-Calcium Fly Ash Geopolymer. Civil Engineering Journal, 10, 252–270. doi:10.28991/CEJ-SP2024-010-013.

[61] Vafaei, M., Allahverdi, A., Dong, P., Bassim, N., & Mahinroosta, M. (2021). Resistance of red clay brick waste/phosphorus slag-based geopolymer mortar to acid solutions of mild concentration. Journal of Building Engineering, 34, 102066. doi:10.1016/j.jobe.2020.102066.

[62] Kohout, J., Koutník, P., Hájková, P., Kohoutová, E., Soukup, A., & Vakili, M. (2023). Effect of Aluminosilicates' Particle Size Distribution on the Microstructural and Mechanical Properties of Metakaolinite-Based Geopolymers. Materials, 16(14), 5008. doi:10.3390/ma16145008.

[63] Jiao, Z., Li, X., Yu, Q., Yao, Q., & Hu, P. (2023). Sulfate resistance of class C/class F fly ash geopolymers. Journal of Materials Research and Technology, 23, 1767–1780. doi:10.1016/j.jmrt.2023.01.131.

[64] Kwasny, J., Aiken, T. A., Soutsos, M. N., McIntosh, J. A., & Cleland, D. J. (2018). Sulfate and acid resistance of lithomarge-based geopolymer mortars. Construction and Building Materials, 166, 537–553. doi:10.1016/j.conbuildmat.2018.01.129.

[65] Lavanya, G., & Jegan, J. (2015). Evaluation of relationship between split tensile strength and compressive strength for geopolymer concrete of varying grades and molarity. International Journal of Applied Engineering Research, 10(15), 35523–35529.

[66] ACI 318. (1999). Building Code Requirements for Structural Concrete. American Concrete Institute (ACI), Farmington Hills, United States.

[67] ACI 363. (1992). State-of-the-Art Report on High Strength Concrete. American Concrete Institute (ACI), Farmington Hills, United States.

[68] Raphael, J. M. (1984). Tensile Strength of Concrete. Journal of the American Concrete Institute, 81(2), 158–165. doi:10.1007/978-3-642-41714-6_200519.

[69] Oluokun, F. A., Burdette, E. G., & Deatherage, J. H. (1991). Splitting tensile strength and compressive strength relationship at early ages. ACI Materials Journal, 88(2), 115–121. doi:10.14359/1859.

[70] Arioglu, N., Canan Girgin, Z., & Arioglu, E. (2006). Evaluation of ratio between splitting tensile strength and compressive strength for concretes up to 120 MPa and its application in strength criterion. ACI Materials Journal, 103(1), 18–24. doi:10.14359/15123.

[71] Gartner, E. (2004). Industrially interesting approaches to "low-CO_2" cements. Cement and Concrete Research, 34(9), 1489–1498. doi:10.1016/j.cemconres.2004.01.021.

[72] Ramujee, K., & Potharaju, M. (2017). Mechanical Properties of Geopolymer Concrete Composites. Materials Today: Proceedings, 4(2), 2937–2945. doi:10.1016/j.matpr.2017.02.175.

[73] Zain, M. F. M., Mahmud, H. B., Ilham, A., & Faizal, M. (2002). Prediction of splitting tensile strength of high-performance concrete. Cement and Concrete Research, 32(8), 1251–1258. doi:10.1016/S0008-8846(02)00768-8.

[74] Bin Ahmed, F., Biswas, R. K., Abid Ahsan, K., Islam, S., & Rahman, M. R. (2021). Estimation of strength properties of geopolymer concrete. Materials Today: Proceedings, 44(1), 871–877. doi:10.1016/j.matpr.2020.10.790.